

Green Thermochemical Modification of Silicon Microparticles for Next- Generation Li-ion Battery Anodes

Ali Abo Hamad

Main supervisors: Assoc. Prof. Jonas Örtegren

Co-supervisors: Dr. Manisha Phadatare

Faculty of Faculty of Science, Technology and Media

Thesis for Licentiate degree in Engineering Physics

Mid Sweden University

Sundsvall, 2025-11-28

Akademisk avhandling som med tillstånd av Mittuniversitetet i Sundsvall framläggs till offentlig granskning för avläggande av teknologie licentiatexamen Fredag, den 28 november, 09:00, C312, Mittuniversitetet Sundsvall. Seminariet kommer att hållas på engelska.

Green Thermochemical Modification of Silicon Microparticles for Next-Generation Li-ion Battery Anodes

© Ali Abo Hamad, 2025

Printed by Mid Sweden University, Sundsvall

ISSN: 1652-8948

ISBN: 978-91-90017-45-6

Faculty of Faculty of Science, Technology and Media
Mid Sweden University, Holmgatan 10, SE-851 70, Sundsvall
Phone: +46 (0)10 142 80 00

Mid Sweden University Licentiate Thesis 212

For my wife, who carried my heart when I was buried in work,
for my family, whose faith lit every dark corridor of research,
and for my friends, who reminded me that life is larger than
any thesis

Acknowledgement

This thesis is the result of many hands, minds, and hearts, and I am deeply grateful for all the support along the way.

My sincere thanks go to Jonas Örtegren, whose generosity, guidance, and friendship paved the road for me. To Manisha Phadatare, thank you for your steady support and for always being a colleague I could also call a friend.

My thanks extend to Daniel Brandell (Uppsala), from the moment I first encountered your work, you have been a compass. Your guidance, network, and deep expertise have shaped how I think and work. To Maria Hahlin (Uppsala), thank you for helping me sharpen my analysis, challenge assumptions, and strengthen every detail of this work.

At Mid Sweden University, Magnus Hummelgård shared invaluable knowledge and brightened this journey through our many coffee-break talks. I am also grateful to Ghadir Razaz and Shahrzad Rastabi for their early support.

To my fellow PhD companions: Luke Bond, Suprokash Hazra, Mohamed Helal, and Rohan Patil, thank you for your friendship, discussions, and laughter, which kept the balance between hard work and good life.

To my parents, Jehad Abo-Hamad and Dunia Alkurdi, your love and prayers are the foundation beneath every step I take.

To my wife, Noor Al Haj Ibrahim, for your patience, love, and belief in me. And to our small family, Nada, Ghena, and Jana, thank you for the joy, warmth and cheer you bring into every day.

To all of you: this work carries your mark as much as mine.

Table of Contents

Abstract	v
Summary in Swedish	vi
List of papers	vii
List of Abbreviations	viii
Preface	x
1 Introduction	1
1.1 Motivation and significance	1
1.2 Research objectives	4
2 Background	5
2.1 Batteries	5
2.2 Conventional anode materials	8
2.2.1 Intercalation-Type Anodes.....	8
2.2.2 Alloying-Type Anodes.....	9
2.2.3 Conversion-Type Anodes	10
2.2.4 Comparative Overview	10
2.3 Silicon as anode material	11
2.3.1 Limitations	12
2.3.2 Strategies to improve silicon anodes.....	17
2.4 Porous Silicon Synthesis and Structural Design	21
2.4.1 Chemical Etching.....	22
2.4.2 Electrochemical Etching	23
2.4.3 Metallothermic Reduction	24
2.4.4 Hydrothermal Synthesis	25
2.4.5 Template-Based Synthesis and Dealloying.....	25
2.5 Structural Features: Isotropy, Anisotropy, and Hierarchical Architectures ...	26
2.6 Toward sustainable approaches.....	27
3 Methodology	28
3.1 Synthesis of porous silicon	29
3.2 Electrode preparation	30

3.3 Characterization techniques	31
4 Results and Discussion	33
4.1 Development of porous silicon microparticles (Paper I)	33
4.2 Integration of porous Si into graphite-based composite anodes (Paper II) ..	40
5 Conclusions and Outlook	41
5.1 Main conclusions	41
5.2 Limitations of the study	42
5.3 Future work.....	43
6 Bibliography.....	45

Abstract

Silicon is a leading candidate for next-generation lithium-ion battery anodes thanks to its high theoretical capacity, yet its use is restricted by severe volume expansion and rapid capacity fading. A further challenge is that many approaches to stabilize Si rely on hazardous or complex syntheses.

This thesis presents a green, hydrofluoric acid-free thermochemical route to engineer porous silicon microparticles using urea as an etching agent. The process combines chemical reactions and mechanical stress from urea decomposition, producing mesoporous networks while maintaining crystalline integrity. Under favorable conditions, surface areas up to $\sim 27 \text{ m}^2 \text{ g}^{-1}$ were achieved, along with stabilizing Si–O and Si–N surface species confirmed by structural and chemical analyses.

Porous silicon was then incorporated into graphite composites for lithium-ion battery anodes. Electrodes with 10-20 wt% porous silicon delivered stable specific capacities of 630-880 mAh g⁻¹ after 100 cycles, more than doubling untreated silicon composites and tripling pure graphite, while maintaining coulombic efficiencies above 98%. Higher silicon loadings caused instability, whereas rate tests showed porous silicon retained $\sim 70\%$ of its capacity at 2C.

These results establish urea-assisted porosification as a sustainable path toward practical silicon anodes and highlight the role of porosity in enabling stable, high-capacity batteries. Future work will focus on optimizing porous silicon as a stand-alone active material and performing postmortem analyses to clarify degradation mechanisms and the role of porosity in electrode stability.

Summary in Swedish

Kisel (Si) är ett lovande anodmaterial för nästa generations litiumjonbatterier (LIB) tack vare sin mycket höga teoretiska kapacitet. Den praktiska användningen begränsas dock av kraftiga volymförändringar under cykling, vilket leder till sprickbildning, instabila gränssnitt och snabb kapacitetsförlust. Dessutom bygger många metoder för att framställa poröst kisel på vätefluoridsyra (HF), vilket innebär miljö- och säkerhetsproblem. I denna avhandling presenteras en grön och skalbar termokemisk metod för att framställa porösa kiselmikropartiklar med hjälp av urea-baserad etsning. Processen kombinerar kemisk reaktivitet och mekanisk stress från ureas fasövergångar vid förhöjd temperatur och ger mesoporösa strukturer samtidigt som kristalliniteten bevaras. Under gynnsamma förhållanden uppnåddes ytor på upp till $\sim 27 \text{ m}^2 \text{ g}^{-1}$, och analyser visade stabiliserande Si-O, och Si-N-bindningar vid ytan. Poröst kisel införlivades i grafitkompositer för elektrokemiska tester. Elektroder med 10-20 vikt% kisel uppvisade stabila kapaciteter på 630-880 mAh g^{-1} efter 100 cykler vid 0,1C, med coulombiska verkningsgrader över 98 %. Detta är mer än dubbelt så mycket som obehandlat kisel och nästan tre gånger så mycket som ren grafit. Högre kiselhalter ledde däremot till försämrad stabilitet. Vid hastighetstester behölls 65-74 % av kapaciteten vid 2C, vilket visar god effekt, och cyklingsprestanda. Arbetet visar att urea-baserad porosifiering är en hållbar metod för att producera funktionella kiselanoder. Framtida studier kommer att fokusera på att optimera poröst kisel som ett fristående aktivt material samt genomföra post mortem-analyser för att förstå degraderingsmekanismer och porositetens betydelse.

List of papers

Paper I

Safe and cost-effective synthesis of porous silicon using Urea: Structural, morphological, and porosity analysis.

Ali Abo-Hamad, Manisha Phadatare, Fredrik Lindgren, Daniel Brandell, Maria Hahlin, Jonas Örtegren

Microporous and Mesoporous Materials, Volume 397, 2025, 113773, ISSN 1387-1811, <https://doi.org/10.1016/j.micromeso.2025.113773>.

Paper II

Porous Structuring of Si Microparticles for Li-Ion Battery Anodes by Urea-Assisted Etching

Ali Abo-Hamad, Manisha Phadatare, Daniel Brandell, Maria Hahlin, Jonas Örtegren

Submitted

List of Abbreviations

a-Si	Amorphous silicon
BET	Brunauer–Emmett–Teller
BJH	Barrett–Joyner–Halenda
CCT	Critical cracking thickness
CNTs	Carbon nanotubes
c-Si	Crystalline silicon
CV	Cyclic voltammetry
CVD	Chemical vapor deposition
DMC	Dimethyl carbonate
EDS	Energy-dispersive x-ray spectroscopy
EIS	Electrochemical impedance spectroscopy
FEC	Fluoroethylene carbonate
HF	Hydrofluoric acid
ICE	Initial coulombic efficiency
LHCEs	Localized high-concentration electrolytes
LIB	Lithium-ion battery
LiFSI	Lithium bis(fluorosulfonyl)imide
Li-M	Lithium-metal alloy
LiTFSI	Lithium bis(trifluoromethanesulfonyl)imide
LTO	Lithium titanate
MACE	Metal-assisted chemical etching
MXene	2d transition-metal carbide/nitride/carbonitrides material
NG	Nanographite
NGE	Nanographite based electrode
Ni-Cd	Nickel-cadmium

Ni-MH	Nickel-metal hydride
PFPI	Pentafluorophenyl isocyanate
PoSi	Porous silicon
PoSi-10/NGE	Porous silicon (10%) on nanographite electrode
PoSi-20/NGE	Porous silicon (20%) on nanographite electrode
PoSi-45/NGE	Porous silicon (45%) on nanographite electrode
PrSi	Pristine silicon
PrSi-10/NGE	Pristine silicon (10%) on nanographite electrode
PrSi-20/NGE	Pristine silicon (20%) on nanographite electrode
PrSi-45/NGE	Pristine silicon (45%) on nanographite electrode
PSD	Particle size distribution
Rct	Charge-transfer resistance
SA	Sodium alginate
SEI	Solid electrolyte interphase
SEM	Scanning electron microscopy
Si	Silicon
Si-220-AP	Atmospheric pressure treatment in a crucible at 220°C
Si-220-HP	High pressure treatment with an autoclave at 220°C
Si-400-AP	Atmospheric pressure treatment in a crucible at 400°C
Si-600-AP	Atmospheric pressure treatment in a crucible at 600°C
Si-800-AP	Atmospheric pressure treatment in a crucible at 800°C
STA	Simultaneous thermal analyzer
TEP	Triethyl phosphate
TGA	Thermogravimetric analysis
XPS	X-ray photoelectron spectroscopy
XRD	X-ray diffraction

Preface

This licentiate thesis summarizes my research conducted at the Department of Engineering Physics, Mid Sweden University, between 2023 and 2025. The overall aim of the work has been to develop environmentally friendly methods for tailoring porous silicon microparticles and to investigate their potential as active materials in lithium-ion battery anodes. The thesis is based on two main studies. The first part focuses on the synthesis of porous silicon through a hydrofluoric acid-free, urea-assisted thermochemical process, highlighting the influence of processing conditions on porosity and surface chemistry. The second part explores the incorporation of these porous silicon particles into graphite-based composite anodes and evaluates their electrochemical performance in half-cell configurations. Together, these studies provide new insights into sustainable routes for silicon modification and their implications for next-generation battery technology. Future work will extend this research toward optimizing porous silicon as a stand-alone active material and conducting postmortem analyses to better understand degradation mechanisms and the role of porosity in cycling stability. The research presented here has been carried out in collaboration with colleagues at Mid Sweden University and Uppsala University. I was responsible for the synthesis of materials, electrode fabrication, electrochemical testing, and structural characterization. The data analysis and interpretation of results were carried out in close collaboration with my co-authors. Writing this thesis has been both challenging and rewarding. It reflects not only the scientific results achieved but also the learning process of working across materials chemistry, electrochemistry, and sustainable energy research.

1 Introduction

1.1 Motivation and significance

The transition toward a sustainable and electrified society relies fundamentally on efficient and scalable energy storage technologies. Renewable sources such as solar and wind are intermittent by nature, generating electricity that must be stored for later use. Among available storage solutions (mechanical, thermal, electrostatic, and chemical), electrochemical storage through batteries stands out for its high efficiency, modularity, and adaptability across applications ranging from portable electronics to electric vehicles and grid balancing.¹ Batteries function as “banks of electricity,” storing excess energy when production exceeds demand and releasing it during peak consumption, thus ensuring the stability and reliability of modern energy systems.

Among battery technologies, lithium-ion batteries (LIBs) dominate current markets owing to their high energy density, long cycle life, and declining manufacturing cost.² Despite these advantages, further progress in LIBs is constrained by the graphite anode, whose theoretical capacity of 372 mAh g⁻¹ limits the total energy density of present-day systems.^{3,4} Overcoming this bottleneck is vital for longer-range electric vehicles, faster charging devices, and more sustainable energy storage solutions.

Silicon (Si) has emerged as one of the most promising next-generation anode materials. It offers a theoretical capacity of 3579 mAh g⁻¹ for the Li₁₅Si₄ phase and up to ~4200 mAh g⁻¹ for the fully lithiated phase (Li₂₂Si₅), nearly ten times higher than graphite. In addition, Si combines natural abundance, low cost, and a low lithiation potential (~0.3 V vs. Li/Li⁺).⁵ These features make Si particularly attractive for future high-

energy LIBs. However, Si suffers from several critical limitations: poor intrinsic conductivity and large volume expansion (~300-360%) during cycling, which cause particle pulverization, unstable interfaces, and rapid capacity fading.⁶ In practice, only small amounts of nanosilicon (5-10 wt%) are typically incorporated into graphite-Si composite anodes,^{7,8} since sub-150 nm particles show better structural stability.^{9,10} However, nanosizing also increases surface area, which intensifies the formation of solid electrolyte interphase (SEI) layer and raises manufacturing cost due to complex silane-based synthesis methods.^{11,12} Thus, the key challenge is not whether Si can provide high capacity, but whether it can do so reliably and sustainably.

Introducing porosity has proven to be an effective way to address these challenges. Internal voids act as mechanical buffers, absorbing strain during lithiation and delithiation, while the porous network facilitates lithium-ion diffusion and helps maintain a stable SEI layer.^{13,14} However, many current porous-Si synthesis techniques still rely on hazardous reagents such as hydrofluoric acid (HF),¹⁵⁻¹⁷ high-temperature processing,¹⁸ or multistep templating methods.¹² HF-based etching, though efficient, poses severe environmental and safety risks, whereas alkaline etching often yields irregular and poorly controlled pore structures in polycrystalline particles.^{19,20} Other HF-free alternatives, such as ionic liquid anodization or templating with costly reagents, remain expensive and difficult to scale.²¹ These limitations underscore the need for a simpler, HF-free, and industrially viable route to produce porous Si.

This thesis introduces a green thermochemical strategy for modifying Si microparticles using urea as an etching agent. Upon heating, urea decomposes into NH₃, HNCO, CO₂, and related species.²²⁻²⁴ These byproducts act through a dual mechanism: chemically etching the Si

surface while simultaneously generating internal porosity through gas evolution. Prior studies on ammonia etching suggest that NH_3 can both etch and passivate Si, allowing for controllable porosity formation without compromising crystallinity.²⁵ Therefore, urea-assisted thermochemical processing represents a promising HF-free, environmentally friendly, and scalable method for synthesizing porous Si.

When porous Si microparticles are integrated into graphite-Si composite electrodes, they combine the mechanical stability of graphite with the high capacity of Si. Preliminary results show that moderate Si loadings significantly increase reversible capacity compared with graphite alone or untreated Si composites, while maintaining high coulombic efficiency. However, excessive Si content still leads to mechanical degradation, emphasizing the importance of balancing porosity, composition, and structural integrity.

The motivation for this research arises from two converging global needs: the demand for higher-energy LIBs that surpass the limitations of graphite and the necessity of sustainable, non-toxic, and scalable synthesis methods. By demonstrating that porous Si can be produced through a green, HF-free thermochemical route and effectively integrated into functional composite anodes, this work contributes to both energy performance and environmental sustainability. It establishes thermochemical modification as a viable platform for next-generation anodes and lays the groundwork for future studies on stand-alone porous Si, complemented by postmortem analyses to reveal how porosity influences lithium transport, structural stability, and electrode degradation during extended cycling.

1.2 Research objectives

The overarching objective of this thesis is to develop a green, scalable strategy for tailoring porous Si microparticles and to evaluate their potential as active materials for next-generation LIB anodes. In particular, the work seeks to address two key challenges: enhancing the energy density of LIBs beyond the limits of graphite and replacing hazardous, HF-based synthesis routes with sustainable alternatives.

The specific objectives are:

- To establish an HF-free thermochemical process for producing porous Si microparticles using urea as an environmentally benign etching agent.
- To investigate the influence of synthesis conditions on porosity, surface chemistry, and structural integrity of the resulting Si particles.
- To incorporate porous Si into graphite-based composite anodes and benchmark their electrochemical performance against graphite and untreated Si composites.
- To evaluate the balance between Si content, porosity, and cycling stability, identifying loading levels that enable high specific capacity while maintaining durability.
- To provide a foundation for future studies on stand-alone porous Si anodes and postmortem analyses aimed at clarifying how porosity contributes to lithium transport, structural stability, and the long-term degradation of electrodes.

2 Background

2.1 Batteries

At their core, batteries are electrochemical cells that convert chemical energy into electrical energy through reversible redox reactions occurring at two electrodes separated by an electrolyte. Depending on reversibility, they are categorized as primary (non-rechargeable) or secondary (rechargeable) systems.²⁶ The historical evolution of secondary batteries has followed a clear trajectory: from the lead-acid battery, introduced in the mid-19th century and still widely used due to its low cost and robustness, to nickel-cadmium (Ni-Cd) and nickel-metal hydride (Ni-MH) systems that offered higher specific energy and longer cycle life.³ However, the growing need for lighter, more durable, and energy-dense power sources for mobile and stationary use ultimately led to the development of lithium-based technologies, which now dominate the market.

LIBs represent the most successful class of secondary batteries to date. Introduced commercially by Sony in the early 1990s, LIBs use lithium ions as charge carriers that shuttle reversibly between two host materials: a carbonaceous anode (typically graphite) and a transition metal oxide cathode.²⁷ This “rocking-chair” mechanism enables high voltage, excellent reversibility, and energy densities far exceeding those of earlier chemistries.²⁸ Over the past three decades, the energy density of LIBs has increased by a factor of three to four, while production costs have dropped by nearly 90%, driving their widespread use in electronics, electric mobility, and stationary storage.^{29,30}

A typical LIB comprises four essential components:

1. Anode: usually graphite, responsible for Li^+ intercalation during charging.
2. Cathode: commonly a layered transition metal oxide (e.g., LiCoO_2 , NMC, LFP) that releases and re-accepts Li^+ during cycling.
3. Electrolyte: a lithium salt (e.g., LiPF_6) dissolved in organic solvents, which facilitates ion transport between electrodes.
4. Separator: a porous polymeric membrane that prevents electrical contact while allowing ionic flow.

During charging, lithium ions migrate from the cathode to the anode through the electrolyte while electrons flow externally through the circuit. The process reverses upon discharge, delivering electrical energy to the external load. A schematic illustration of the working principle and main components of a lithium-ion battery is presented in Figure 2.1.

The success of LIBs stems from their high efficiency, light weight, and adaptability to various form factors, from coin cells to large battery packs. These advantages have made them the cornerstone of the ongoing electrification of transportation and renewable energy integration. However, the massive global deployment of LIBs, projected to exceed 1 TWh of installed capacity by 2030, introduces new challenges related to resource availability, cost, and sustainability.^{26,31} The dependence on critical elements such as lithium, cobalt, and nickel, along with the use of flammable organic electrolytes, raises concerns about long-term supply security, safety, and environmental impact.³²

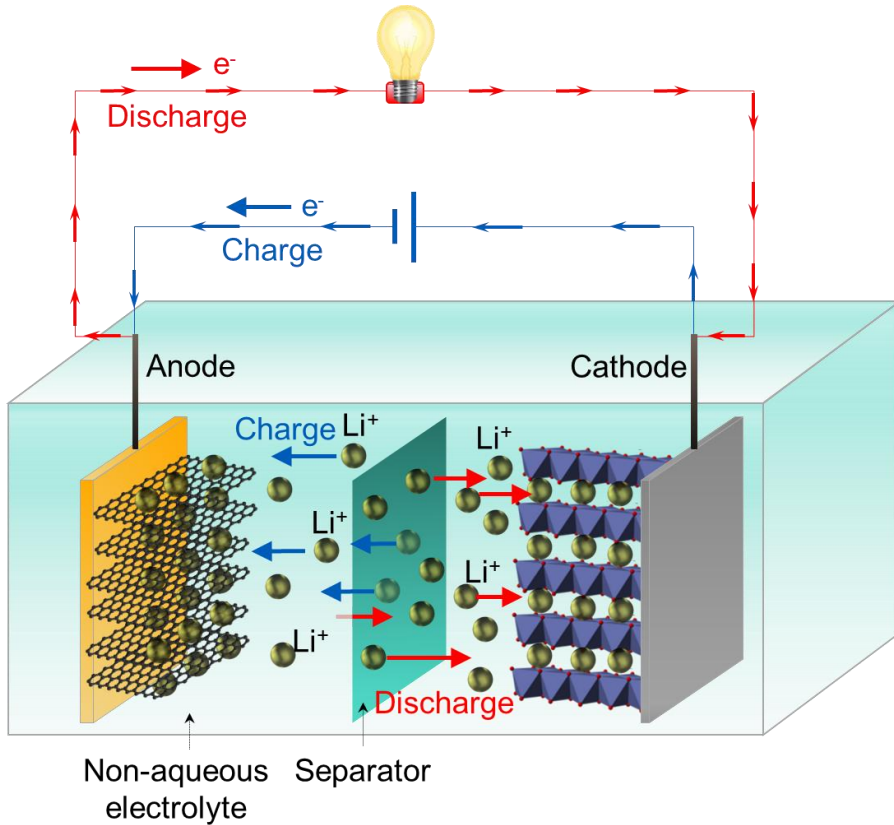


Figure 2. 1 Schematic illustration of a lithium-ion battery showing the movement of Li^+ ions and electrons during charge and discharge.

Consequently, current battery research is increasingly directed toward sustainable and high-performance materials. Efforts include developing cobalt-free cathodes³³ and engineering advanced anode materials with higher capacity than graphite. In this context, Si-based anodes have emerged as particularly promising due to their exceptional theoretical capacity and compatibility with existing LIB manufacturing platforms. The continued evolution of LIB technology, both in efficiency and sustainability, depends on progress in electrode materials. Improvements are needed for both the cathode, where reducing cobalt content is essential, and the anode, where silicon offers

major potential gains in capacity. This thesis focuses on the anode side, aiming to enhance its performance and sustainability.

2.2 Conventional anode materials

The anode plays a critical role in LIBs as the host for lithium-ion insertion during charging. Its electrochemical characteristics largely determine the battery's energy density, rate capability, and long-term stability. A suitable anode should combine a low lithiation potential, high reversible capacity, good electronic and ionic conductivity, and structural stability during repeated cycling.³⁴

Conventional anode materials for LIBs are generally classified according to their lithium storage mechanisms into three main categories: intercalation-type, alloying-type, and conversion-type systems.³⁵ Each class involves a distinct mode of lithium accommodation within the host, which strongly influences its electrochemical behavior, energy density, and durability. In addition, some disordered carbons (e.g., hard carbon) exhibit a mixed intercalation-adsorption mechanism and can be regarded as a transitional subclass of intercalation materials.³⁶

2.2.1 Intercalation-Type Anodes

Among all anode materials, carbon-based systems remain the commercial standard because of their stability, safety, and mature manufacturing processes.

Graphite has long dominated LIBs owing to its layered structure that allows reversible Li^+ intercalation through a staging process down to LiC_6 , providing a theoretical capacity of 372 mAh g^{-1} at about 0.1 V vs Li/Li^+ .^{37,38} Its high reversibility and flat potential profile enable excellent cycle life and coulombic efficiency.

Nevertheless, its relatively low capacity limits the overall energy density, and at high charge rates or low temperatures lithium plating can occur because the graphite potential approaches that of metallic lithium.³⁹

Beyond graphite, hard carbon (non-graphitizable) and soft carbon (partially graphitizable) materials have been explored. Hard carbon contains turbostratic disorder and closed nanopores that store Li⁺ both between graphene layers and within pores, yielding capacities up to 400-500 mAh g⁻¹,⁴⁰ though with lower initial coulombic efficiency (ICE) due to irreversible Li trapping.⁴¹ Soft carbon offers better conductivity and easier graphitization but similar capacities to graphite.⁴² Disordered carbons, such as hard carbon, can therefore be viewed as a special subclass of intercalation materials where lithium storage occurs by both intercalation and adsorption, resulting in enhanced low-temperature performance.

Another important intercalation-type anode is lithium titanate (Li₄Ti₅O₁₂, LTO), which operates at ~1.55 V vs Li/Li⁺. LTO exhibits excellent safety and exceptional cycle life because of its negligible lattice strain (“zero-strain” property).^{43,44} However, the high potential reduces full-cell energy density, and its low conductivity necessitates doping or conductive coatings. LTO is therefore well suited for high-power or grid-storage applications where safety and cycle life outweigh energy density.

2.2.2 Alloying-Type Anodes

Alloying materials such as Sn, Sb, Al, and particularly Si store Li through the formation of lithium-metal (Li-M) alloys, reaching theoretical capacities of 500-4000 mAh g⁻¹.⁴⁵ These reactions, however, involve 200-400% volume expansion, causing mechanical fracture and

unstable SEIs. Nanostructuring, conductive matrices, and carbon coatings have been applied to mitigate these effects.^{45,46}

Si, the most prominent member of this group, will be discussed in detail in Section 2.3.

2.2.3 Conversion-Type Anodes

Conversion anodes, including transition-metal oxides, sulfides, nitrides, and phosphides, react with lithium according to:



They deliver capacities of 600-1200 mAh g⁻¹ using abundant elements.⁴⁷

However, these materials suffer from large voltage hysteresis, poor conductivity, and structural reconstruction during cycling, limiting their energy efficiency and cycle life.⁴⁸

Nanoscale engineering and conductive carbon scaffolds can enhance their electrochemical reversibility but often increase synthesis complexity and cost.

2.2.4 Comparative Overview

Conventional anode materials thus offer diverse trade-offs among capacity, potential, and structural stability. Graphite continues to dominate the commercial market because of its reliability and cost-effectiveness, while hard carbons and alloying-type materials promise higher capacities and LTO ensures exceptional safety.

However, none of these materials simultaneously provide high capacity, low potential, and long-term stability. These limitations have motivated hybrid architectures that combine complementary mechanisms, most notably, the incorporation of Si within graphite matrices to balance energy density and stability.

A comparative summary of the main anode material classes is presented in Table 2. 1, highlighting their representative materials, capacities, operating potentials, and key performance considerations.

Table 2. 1 Summary of main anode material types and their electrochemical characteristics, highlighting representative materials, typical capacity, potential, and main advantages and limitations.^{37,41,43,45,48}

Mechanism	Example materials	Capacity (mAh g ⁻¹)	Potential (V vs Li/Li ⁺)	Key features	Limitations
Intercalation-type carbons	Graphite, hard carbon	372-500	0.05-0.8	Mature technology, good conductivity, safe	Limited energy density, SEI formation
Intercalation oxides	Li ₄ Ti ₅ O ₁₂	175	1.55	Zero-strain, excellent cycle life	Low voltage, low energy density
Alloying	Si, Sn, Sb, Ge	500-4000	0.3-0.6	Very high capacity, abundant	Severe volume change, unstable SEI
Conversion	Fe ₂ O ₃ , Co ₃ O ₄ , MoS ₂	600-1200	0.6-1.5	High theoretical capacity	Voltage hysteresis, poor conductivity

Overall, the evolution of anode materials highlights the ongoing trade-off between energy density, safety, and durability. This balance continues to drive research toward Si-based systems, discussed in the following section.

2.3 Silicon as anode material

Si is the leading alloy-type anode for next-generation Li-ion batteries because it can host up to ~3.75-4.4 Li per Si forming Li₁₅Si₄ or Li₂₂Si₅

phases, and delivering a theoretical capacity of ~3579-4200 mAh g⁻¹, roughly 10 times that of graphite (372 mAh g⁻¹).⁴⁹ Its operating potential (~0.37 V vs. Li/Li⁺) is slightly higher than graphite, which helps mitigate Li plating and improves safety.⁵⁰ Its natural abundance (~27.7 % of Earth's crust) and mature processing technologies further make Si suitable for large-scale manufacturing.^{51,52}

Historically, the Li-Si alloying mechanism was already identified in the 1970s, when high-temperature sulfide batteries revealed Li-Si alloy formation and the sequence of lithiation phases (Li₁₂Si₇, Li₇Si₃, Li₁₃Si₄, Li₂₂Si₅).^{53,54} Yet, at ambient conditions early work noted low reversibility, now linked to massive volume changes and unstable interfaces that fracture the active phase and continuously rebuild the SEI layer. This coupling of electrochemistry and mechanics defines modern Si anode design.

2.3.1 Limitations

i. Mechanical degradation from volume expansion

Si undergoes a ~300-360% volume expansion during full lithiation.⁵⁵ The insertion of Li⁺ generates a concentration gradient across the Si particle, producing complex internal stresses: compressive hoop stress develops in the outer lithiated shell, while the inner unlithiated core experiences tensile stress. Upon delithiation, the stress direction reverses, leading to the accumulation of cyclic strain energy and, ultimately, crack initiation and propagation once the local stress exceeds the particle's cohesive strength.^{56,57} These repeated expansion-contraction cycles cause particle pulverization, loss of electronic contact with the conductive matrix, and progressive structural disintegration of the electrode. Simultaneously, the SEI ruptures and reforms continuously, exposing fresh Si surfaces to electrolyte reduction. This ongoing reaction consumes both Li⁺ and solvent

species, resulting in a low ICE ($\approx 70\text{-}85\%$) and accelerated long-term capacity fading.^{58,59} Even a small coulombic inefficiency of $\sim 0.1\%$ per cycle can cumulatively deplete the cyclable lithium reservoir over extended operation.⁶⁰ Figure 2. 2 illustrates the volume expansion of a Si particle during lithiation, showing crack formation and deformation of the surrounding SEI layer.

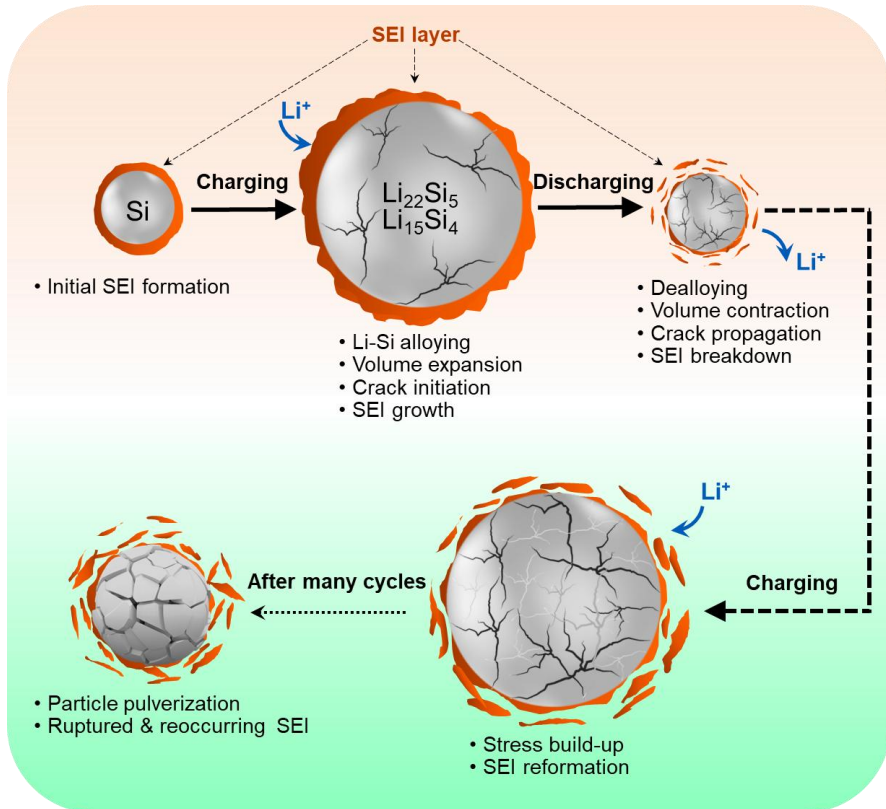


Figure 2. 2 Schematic illustration of silicon particle volume expansion, surface cracking, and SEI layer rupture during lithiation/delithiation in lithium-ion batteries.

Phase-dependent mechanical behavior (crystalline vs. amorphous Si)

Crystalline and amorphous Si exhibit distinct degradation behaviors. In crystalline Si (c-Si), fracture typically occurs during lithiation, driven by the sharp two-phase boundary between lithiated and

unlithiated regions. In contrast, amorphous Si (a-Si) accommodates strain more uniformly during lithiation but suffers greater mechanical degradation upon delithiation, when contraction of the outer lithiated layer imposes tensile stress on the amorphous network.^{61,62} These structural differences explain why pulverization of c-Si is commonly observed during lithiation, while a-Si tends to degrade during Li extraction. Such chemo-mechanical instability is a primary cause of poor cycling stability and irreversible capacity loss in Si anodes. Consequently, pure Si is rarely used directly as an active material. These observations highlight the need for structural or compositional modification to accommodate strain and prevent catastrophic fracture.⁶³

Particle size effect on fracture and stability

When the particle radius falls below a critical size, approximately 150 nm for c-Si nanoparticles, and ≈ 300 nm for nanowires, fracture can be averted, since the elastic strain energy released upon cracking becomes smaller than the surface energy required to create new surfaces.^{64,65} In other words, at nanoscale dimensions, elastic deformation dominates over brittle failure, and the energy balance favors stability rather than crack propagation. This mechanical stabilization, however, comes at the penalty of accelerated surface energy accumulation, which amplifies side reactions with the electrolyte and leads to extensive SEI formation.⁶⁶ Despite mitigating fracture at the subparticle level, size reduction does not eliminate Si's intrinsic volume change.^{56,57,62} Even below the critical size, rapid Li⁺ diffusion gradients can induce localized stress fields that cause pore nucleation or structural coarsening, particularly under high C-rates.⁶⁷ In Si nanoparticles (< 50 nm), vacancy clustering during delithiation was found to generate internal porosity, which gradually evolves into highly porous,

disconnected frameworks with poor electrical integrity and rapid capacity decay.^{67,68}

The phase structure also plays a decisive role in size-dependent stability. a-Si, with a fracture toughness of $\approx 5.8 \text{ J m}^{-2}$ and a volumetric expansion of $\sim 280 \%$, can tolerate larger particle sizes (up to $\approx 870 \text{ nm}$) without mechanical failure.^{69,70} In contrast, c-Si, exhibiting lower toughness ($0.73\text{-}0.89 \text{ MPa}\cdot\text{m}^{1/2}$) and a higher Young's modulus ($\sim 189 \text{ GPa}$), typically fractures during lithiation due to the formation of a sharp two-phase boundary between lithiated and unlithiated regions.⁷⁰ a-Si undergoes more homogeneous lithiation, enabling gradual strain accommodation during Li insertion and delaying crack initiation.^{61,62} However, upon delithiation, tensile stresses can still accumulate and induce microcracking, emphasizing that nanosizing and amorphization mitigate but do not remove mechanical degradation.^{61,71} Beyond size and structure, introducing controlled porosity within Si architectures has proven highly beneficial. Engineered internal voids, either generated through etching, templating, or partial dealloying, provide free volume to absorb expansion and alleviate interparticle stress. This porous design enhances mechanical resilience and facilitates electrolyte access but must be carefully optimized to avoid excessive surface reactivity.^{72,73} Studies consistently show that nanostructured porous Si combined with uniform surface coatings achieves the most stable performance, as porosity allows volumetric buffering, while coatings suppress side reactions and stabilize the SEI layer.^{74,75} While nanosizing and controlled porosity reduce fracture and improve stress tolerance, their optimization remains critical, since excessive surface area exacerbates SEI growth. These size-surface trade-offs guide many of the engineering strategies discussed in Section 2.3.2

ii. Transport-mechanics coupling and electrical isolation

Si's inherently low electrical conductivity ($\sim 10^{-5}$ S cm⁻¹) hinders uniform charge distribution, and its limited ionic transport produces gradients in Li concentration across the particle.^{76,77} These gradients amplify the stress differential between the lithiated surface and unlithiated core, reinforcing crack propagation under cycling. Once fractures occur, electrical pathways break and the newly isolated fragments rapidly lose capacity, giving rise to the "electrical isolation" problem characteristic of pure Si anodes.⁷⁸

iii. Interfacial instability and SEI evolution

Operating at low potentials causes Si to initiate electrolyte reduction early, forming an SEI layer that evolves continuously with cycling. Large volume oscillations fracture the SEI, prompting repeated reformation and continuous consumption of Li⁺ and electrolyte.^{79–85} Progressive SEI thickening increases impedance, while decomposition products can fill surface pores and hinder Li⁺ ion transport. Even with additives such as fluoroethylene carbonate (FEC), thick-film Si electrodes still experience stress-induced interphase cracking unless the SEI is mechanically reinforced.^{81,86,87}

This unstable interfacial chemistry, coupled with mechanical stress, underpins the rapid impedance growth and fading observed in most high-capacity Si anodes.

iv. Processing and practical constraints

While nanostructuring alleviates mechanical damage, it introduces new challenges at the electrode level. Low tapped density of nanoscale Si limits volumetric energy density, and severe electrode swelling during cycling compromises adhesion and packaging.⁷⁸ Additionally, the critical cracking thickness (CCT) during slurry casting restricts the achievable loading of Si-rich electrodes.⁸⁸ At elevated temperatures

(150-300 °C), reactions between lithiated Si, organic SEI species, and carbonate solvents become exothermic, potentially triggering thermal runaway.⁸⁹ These factors underscore the gap between laboratory performance and practical cell integration.

2.3.2 Strategies to improve silicon anodes

Given the severe chemo-mechanical degradation, interfacial instability, and transport limitations discussed in Section 2.3.1, extensive research has focused on strategies to stabilize Si anodes. These approaches can be categorized according to the scale of intervention, from the intrinsic Si particle to the full electrochemical system, each addressing a distinct degradation mechanism.

i. Silicon-level engineering

- **Nanoscaling and size optimization**

Because Si fractures when its dimensions exceed the critical radius,^{69,70} reducing particle size into the nanoscale regime enables elastic accommodation of strain and suppresses cracking, as discussed in Section 2.3.1.⁹⁰ Experimental studies show that nanostructuring effectively delays fracture and maintains electrical contact during cycling. However, excessively small particles increase surface area and side reactions,⁶⁷ demanding a careful balance between mechanical stability and interfacial control.

- **Prelithiation and phase preconditioning**

Prelithiating Si, either electrochemically, chemically, or mechanically, forms Li_xSi or $\alpha\text{-Si}$ phases before full cycling, which helps to reduce the first-cycle irreversible loss and alleviate stress from phase transformations.⁸⁸ Contact prelithiation in electrolytes, composed of dimethyl carbonate and 1.0 M lithium bis-(trifluoromethanesulfonyl)imide (LiTFSI/DMC), forms a mixed ion-electron conductor layer that preserves electronic connectivity and

pushes the ICE up to $\approx 98\%$ in full cells.⁹¹ Similarly, pre-amorphization of c-Si can soften lithiation pathways and improve mechanical.⁹²

- **Porosity and internal void design**

Porosity engineering provides one of the most effective structural solutions to the intrinsic expansion problem. Introducing controlled internal voids reduces the effective modulus, provides free volume for expansion, and creates continuous ion-diffusion pathways.⁹³ Porous Si frameworks, comprising bicontinuous nanoligaments or mesoporous networks, allow isotropic swelling within pores while preserving a mechanically robust skeleton for electron and ion transport. For instance, “ant-nest-like” porous Si derived from Mg-Si dealloying retained $> 90\%$ of its capacity after 1000 cycles when carbon-coated, with minimal electrode swelling and energy density of 502 Wh kg^{-1} in full cells with NMC111.⁹⁴

Porosity therefore stands as a unifying design principle, providing mechanical compliance, shortened diffusion paths, and improved interfacial stability, making it a central focus of this thesis.

ii. Interface and surface-level engineering

Because the Si surface directly governs SEI formation and electron leakage, engineering this interface is critical to suppress side reactions and mechanical fracture.

- **Oxide coatings and artificial SEI layers**

Ultrathin oxides such as SiO_2 , Al_2O_3 , and HfO_2 have been used as conformal coatings to act as artificial SEI layers.⁶⁴ SiO_2 coatings ($\sim 7 \text{ nm}$) balance Li^+ transport with surface passivation,⁹⁵ while Al_2O_3 provides higher fracture toughness ($2.7\text{-}4.2 \text{ MPa m}^{1/2}$), HF resistance, and promotes LiF-rich SEI formation.⁹⁶⁻¹⁰² HfO_2 coatings offer outstanding chemical stability and suppressed parasitic reactions, achieving ICE $\approx 79\%$ and $\sim 70\%$ capacity retention after 100 cycles.¹⁰³ These coatings

act as mass-transport regulators and mechanical clamps, preserving the integrity of the Si particle during cycling.

- **Carbon and hybrid shells**

Amorphous carbon, graphene, carbon nanotubes (CNTs), and MXenes have been employed as conductive and flexible shells to enhance electron transport while buffering mechanical stress.^{64,104,105} For example, MXene@SiNPs@N-carbon foam retained ≈ 857 mAh g⁻¹ after 500 cycles and delivered ≈ 433 Wh kg⁻¹ in full cells.¹⁰⁶ Similarly, Zeolitic-derived carbon cages around Si reduced the charge-transfer resistance from 542 Ω to 189 Ω and maintained > 1000 mAh g⁻¹ after rate cycling.¹⁰⁷

- **Yolk-shell and hollow architectures**

Yolk-shell designs can be viewed as engineered interfacial systems, where a deliberate void space separates the Si core (“yolk”) from an outer shell of carbon or oxide. This void buffers ≈ 300 % expansion and maintains a stable lateral SEI on the shell surface. Such structures typically sustain > 80 % capacity after 500-1000 cycles at high rates.¹⁰⁸

- **Artificial and polymeric SEI films**

Beyond inorganic coatings, polymeric films, such as polyimides, polydopamine,¹⁰⁹ or ion-conductive gels,¹¹⁰ are used to pre-form flexible SEI layers that reduce electrolyte consumption and enhance mechanical cohesion. These layers stabilize the dynamic Si-electrolyte interface under large volumetric changes.

iii. Electrode-level engineering

The performance of Si cannot be decoupled from the overall electrode structure, where conductive networks, binders, and active/inactive phase balance govern mechanical and electrochemical stability.

- **Conductive additives and architecture**

A homogeneous distribution of conductive carbon ensures continuous electron pathways as Si expands and contracts. Hierarchical designs

combining micro- and nanoscale porosity also facilitate electrolyte access and mitigate internal stress.

- **Graphite inclusion and composite design**

Embedding Si nanoparticles within a graphite matrix yields a graphite-Si composite that combines the high capacity of Si with the mechanical resilience and conductivity of graphite. The graphite framework provides continuous percolation, high tapped density, and buffers mechanical strain.¹¹¹ In particular, graphite-Si-C/TiO₂ composites achieved ICE \approx 80-83 %, tapped density \approx 0.82 g cm⁻³, and stable capacities near 920 mAh g⁻¹ for 900 cycles, corresponding to \approx 288 Wh kg⁻¹ in full cells.¹¹² Graphite's layered structure also smooths potential profiles, minimizing local Li plating.

- **Binders**

Elastic and self-healing binders maintain electrode cohesion during repeated volume changes. Examples include polyrotaxane-polyacrylic acid networks that dissipate mechanical strain and retain \approx 85 % capacity after 370 cycles,¹¹³ and MXene-based conductive binders enabling unusually thick electrodes (\approx 450 μ m, 23 mAh cm⁻²) without delamination.¹¹⁴ Such binders are particularly relevant for porous-Si and G-Si industrial coatings.

iv. Cell-level and electrochemical-environment optimization

Even with optimized materials, electrochemical parameters strongly influence stability.

- **Electrolytes and additives**

FEC remains the benchmark additive, forming LiF-rich SEI that enhances modulus and mitigates crack propagation in thick films.^{81-84,115} Localized high-concentration electrolytes (LHCEs), such as lithium bis(fluorosulfonyl)imide (LiFSI) in triethyl phosphate (TEP)/FEC, improve safety (non-flammability) and maintain > 90 %

capacity after 600 cycles at C/2.¹¹⁶ Polymer electrolytes like pentafluorophenyl isocyanate (PFPI) form flexible SEI but may reduce LiF content.¹¹⁷

- **Operating parameters**

Limiting the potential window (typically 0.05-1.0 V vs Li/Li⁺) minimizes deep lithiation and associated stress.¹¹⁸

Gradual current-rate ramping during formation cycles promotes uniform SEI growth and reduces localized fracture.¹¹⁹

2.4 Porous Silicon Synthesis and Structural Design

Porous Si has emerged as one of the most effective architectures for mitigating the chemo-mechanical degradation of Si anodes, offering free volume for expansion, reduced diffusion distances, and robust electron/ion transport networks. The design and synthesis of porous Si can be broadly divided into top-down and bottom-up approaches, each enabling distinct control over pore morphology, distribution, and connectivity. The resulting structures, ranging from isotropic sponge-like frameworks to anisotropic mesochannels, strongly influence lithiation dynamics, mechanical resilience, and electrochemical performance.¹²⁰ Figure 2. 3 shows the classification of porous Si production methods with major routes including etching, metallothermic reduction, hydrothermal synthesis, template-based synthesis, and dealloying.

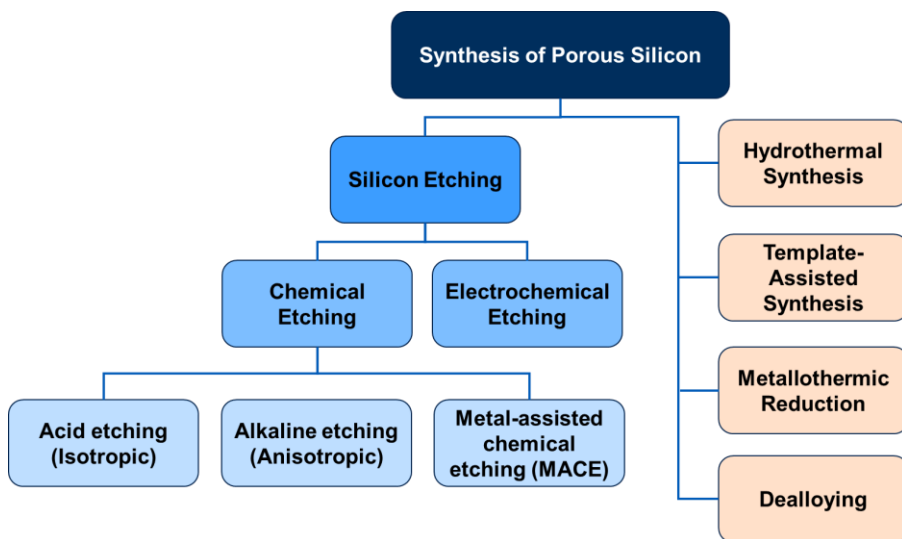


Figure 2. 3 Hierarchical classification of porous silicon production routes.

2.4.1 Chemical Etching

Chemical etching of Si relies on the dissolution of Si in corrosive fluids, primarily HF, sometimes with oxidants, or alkaline solutions, yielding various porous morphologies. These methods can be further classified by whether they produce isotropic (direction-independent) or anisotropic (directionally selective) pore structures.

2.4.1.1 Isotropic Acidic Etching

Isotropic etching with acids, especially mixtures of HF and oxidants such as HNO_3 , removes Si non-preferentially, forming “sponge-like” networks of randomly interconnected pores.^{121–123} This produces a high surface area, highly disordered porous structure typical of microporous and mesoporous Si.

For example, stain etching and wet chemical etching of SiO_2 -derived Si nanoparticles yield thin-walled, hollow Si particles capable of withstanding significant strain during cycling.^{124,125} These architectures accommodate volume expansion and support high specific capacities,

though their high reactivity and surface area may accelerate SEI formation and side reactions.

2.4.1.2 Anisotropic Alkaline Etching

In contrast, anisotropic etching, using alkaline solutions like KOH or NaOH, proceeds along specific crystallographic directions. The result is the formation of well-aligned, faceted pores, trenches, or microchannels.^{126,127} While less common in battery research, these anisotropic etching methods can yield highly ordered, directionally controlled pore architectures, potentially advantageous for tailored electrode design.

2.4.1.3 Metal-Assisted Chemical Etching (MACE)

A special subclass is metal-assisted chemical etching, in which a noble metal catalyst (e.g., Ag) is deposited on the Si surface and the sample is then immersed in an HF/H₂O₂ solution.¹²⁸ The presence of the metal dramatically increases local etch rates, resulting in vertically aligned, anisotropic pores or nanowires. Such architectures offer high electrolyte access, short diffusion paths, and increased tolerance to volume changes.

2.4.1.4 Structural Consequences

The chemical etching route allows fine control over pore size and volume but can generate harmful byproducts and defects, and may introduce impurities or non-uniformities in pore size. Uniform mesoporous shells and hollow core-shell morphologies have been shown to buffer expansion and promote long-term stability, but challenges remain in large-scale application and SEI management.¹²⁹

2.4.2 Electrochemical Etching

Electrochemical etching uses an external electrical bias to drive Si dissolution in HF-based electrolytes. The process allows highly

tunable control over pore size, porosity, and depth by adjusting current density, voltage, and etching time.^{120,130–132}

Depending on the substrate orientation and etching conditions, the resulting porous structure may be isotropic, characterized by random sponge-like pores, or anisotropic, featuring vertically aligned channels. Electrochemically etched mesoporous Si sponges have shown a strong ability to accommodate volume expansion, suppress particle fracture, and sustain stable cycling. The modulation of current density enables tailored pore architectures that optimize ion transport and mechanical integrity. However, this method requires high-purity, conductive Si wafers and specialized equipment, while generating hazardous gaseous byproducts, all of which constrain its scalability.

2.4.3 Metallothermic Reduction

Metallothermic reduction, especially magnesiothermic reduction, converts SiO₂ (often from low-cost sources like rice husk ash) into elemental Si using magnesium at elevated temperatures, followed by acid washing to remove byproducts such as MgO and expose the porous structure.^{133–137}

This method enables the formation of hierarchical porous Si with macroporous, mesoporous, or fibrous morphologies, depending on the precursor characteristics and reaction parameters. Several modified approaches have been developed, including Zn-assisted magnesiothermic reduction,¹³⁴ which improves control over porosity and mitigates particle aggregation, as well as microemulsion-assisted synthesis for producing monodisperse Si nanospheres.¹³⁸ Despite its versatility, the highly exothermic nature of the reduction process can hinder precise control of pore size and distribution. Nevertheless, the resulting three-dimensional interconnected porous Si exhibits remarkable tolerance to volumetric strain and delivers high and stable

capacities. Safety concerns related to reaction exothermicity and the management of residual impurities remain significant challenges for large-scale implementation.

2.4.4 Hydrothermal Synthesis

Hydrothermal synthesis dissolves and reprecipitates Si species under high temperature and pressure, sometimes in the presence of surfactants that guide nanoparticle aggregation into porous networks.^{138–142}

This method can generate a wide range of architectures, including honeycomb-like Si, nanowires, hollow nanospheres, and monodispersed nanoporous Si, with morphology tunable through reaction temperature, time, and precursor composition. Si produced by hydrothermal routes typically exhibits high crystallinity, mechanical robustness, and adjustable porosity. The process is comparatively clean and environmentally benign; however, its scalability is limited by batch-to-batch variability and the requirement for sealed, high-pressure reactors. Structurally, the formation of Si nanospheres and nanowires allows uniform stress distribution, minimizes fracture caused by volume expansion, and contributes to improved electrochemical cycling stability.

2.4.5 Template-Based Synthesis and Dealloying

Template-based synthesis employs a sacrificial template, such as silica spheres or metallic frameworks, which is infiltrated or coated with a Si precursor and subsequently removed to leave a negative replica of the original structure.^{143–147}

Depending on the type of template used, this approach can be categorized into hard templating, utilizing materials such as mesoporous silica or dealloyed metals, and soft templating, which relies on block copolymers or organic assemblies. Dealloying of Si-rich

alloys followed by selective etching can also yield porous Si frameworks with tunable porosity. This method offers exceptional control over pore size, geometry, and connectivity, enabling the fabrication of highly ordered, anisotropic, or hierarchical porous architectures. However, the complexity and cost associated with template preparation and removal, along with the risk of impurity introduction during processing, present significant challenges for large-scale implementation.

2.5 Structural Features: Isotropy, Anisotropy, and Hierarchical Architectures

Regardless of preparation route, the structure of porous Si, specifically, whether the porosity is isotropic or anisotropic, and whether the material is monomodal or hierarchical, crucially impacts battery performance.

Isotropic Porosity: Produced mainly by acid etching, stain etching, or some hydrothermal methods, featuring randomly interconnected, “sponge-like” pores. Provides uniform buffering space for expansion, but may be prone to side reactions due to high surface area.^{124,125,141,148–}

150

Anisotropic Porosity: Generated by alkaline etching, MACE, or template synthesis, yields aligned pores or channels, allowing rapid, directional Li^+ transport and efficient buffering of volume changes.^{128,129,143,144,151}

Hierarchical Porosity: Combining micro-, meso-, and macropores can harness the strengths of each, micropores for capacity, mesopores for transport, macropores for expansion buffering and electrolyte reservoir. Hierarchical 3D networks maximize utilization and stability.^{94,129,138,139,152}

Pore connectivity (“pore openness ratio”) is as important as size, high connectivity ensures continuous access to internal Si, prevents “dead volume”, and supports robust cycling.¹²⁰

2.6 Toward sustainable approaches

Although structural and interfacial engineering have advanced Si-based anodes, achieving sustainability and scalability remains essential for their widespread adoption. Recent efforts focus on green, HF-free synthesis routes that minimize environmental impact while maintaining performance. Among these, the urea-assisted thermochemical approach developed in this work offers a safe and energy-efficient pathway for producing porous Si through in-situ reactions at moderate temperatures, eliminating corrosive HF use. In parallel, renewable silica feedstocks such as rice husks, diatoms, and other agricultural residues enable low-cost, circular-economy routes to high-capacity porous Si via magnesio- or aluminothermic reduction.¹⁵³ Complementary low-energy fabrication techniques, including mechanical milling, sol-gel, spray-drying, and mild CVD, further reduce process intensity and remain compatible with standard industrial electrode manufacturing.¹⁵⁴ Industrial developments increasingly converge toward graphite-Si composites with optimized surface chemistries and electrolytes as near-term solutions for high-energy lithium-ion cells.¹¹¹ Integrating porous Si within conductive graphite matrices, as pursued in this thesis, thus represents a sustainable and commercially aligned strategy for next-generation anodes.

3 Methodology

This chapter describes the experimental methods used in this work, beginning with the thermochemical synthesis of porous Si, followed by electrode fabrication and electrochemical characterization. The overall workflow is summarized in Figure 3.1.

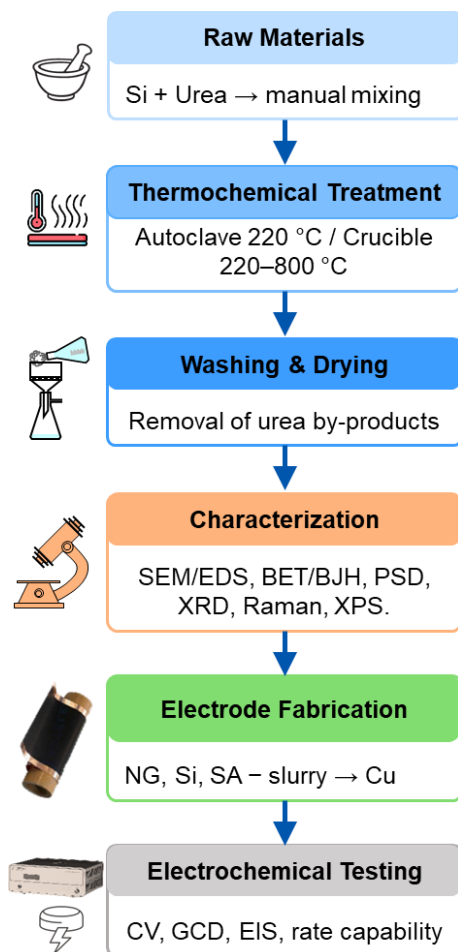


Figure 3. 1 Schematic representation of the experimental workflow for the synthesis, characterization, and electrochemical evaluation of porous silicon microparticles and composite electrodes.

3.1 Synthesis of porous silicon

Metallurgical-grade polycrystalline Si microparticles (SicoMill Grade 2E, purity 98-99%, Vesta Si Sweden AB, Sweden) were used as the starting material without additional purification. Their average particle size was $\sim 5 \mu\text{m}$, with a Brunauer-Emmett-Teller (BET) surface area of $2.3 \text{ m}^2 \text{ g}^{-1}$ and negligible initial porosity. Urea (ACS grade, $\geq 99.5\%$, Sigma-Aldrich) served as the etching agent.

Si microparticles were blended with urea in a 1:2 weight ratio (Si:urea) using an agate mortar and pestle for 10 min to ensure homogeneity. The mixture was then subjected to thermochemical treatment either under high pressure (autoclave) or atmospheric pressure (ceramic crucible) in a programmable furnace (Nabertherm). A two-step heating protocol was applied: heating to $135 \text{ }^\circ\text{C}$ at $5 \text{ }^\circ\text{C min}^{-1}$ and holding for 1 h to melt urea and facilitate infiltration, followed by heating to the target temperature ($220\text{-}800 \text{ }^\circ\text{C}$) at $10 \text{ }^\circ\text{C min}^{-1}$ and maintaining for 12 h.

Two conditions were investigated:

- High-pressure treatment (Si-220-HP): carried out at $220 \text{ }^\circ\text{C}$ in a PTFE-lined autoclave (25-100 mL capacity) to confine decomposition gases.
- Atmospheric-pressure treatments (Si-220-AP, Si-400-AP, Si-600-AP, Si-800-AP): performed in ceramic crucibles at $220\text{-}800 \text{ }^\circ\text{C}$.

After thermal treatment, all samples were thoroughly washed with boiling deionized water to remove residual urea by-products (e.g., biuret, cyanuric acid), filtered, and dried. This washing was essential for low-temperature samples where incomplete decomposition could

leave residues. The washed products were designated as follows: Si-Pristine, Si-220-HP, Si-220-AP, Si-400-AP, Si-600-AP, and Si-800-AP.

For subsequent electrode studies (section 3.2), the Si-220-HP sample was selected as the representative porous Si material due to its balanced porosity and structural integrity.

3.2 Electrode preparation

Composite electrodes were fabricated using nanographite (NG), porous or pristine Si, and sodium alginate (SA) binder. NG was produced via large-scale liquid-phase shear exfoliation of expanded graphite, yielding a mixture of graphene, few-layer graphene, and graphite nanoplatelets. SA (Fisher Scientific) was chosen as a water-soluble binder with high mechanical strength and abundant carboxyl groups, known to enhance electrode stability and coulombic efficiency. Copper foil (25 μm , 99.9%, Goodfellow) served as the current collector.

Electrode slurries were prepared by dispersing the solid components in deionized water (30 mL) and homogenizing with an Ultra-Turrax T25 shear mixer at 10,000 rpm for 1 h. Slurry formulations corresponded to mass ratios of NG:Si:SA = 9:0:1, 8:1:1, 7:2:1, and 4.5:4.5:1, yielding electrodes with 0, 10, 20, and 45 wt% Si, respectively. Both pristine Si (PrSi) and porous Si (PoSi, i.e., Si-220-HP) were used, producing a total of seven electrode types (Table 3.1).

The resulting slurries were cast onto Cu foil, dried at room temperature for 24 h, and punched into 16 mm diameter disks with a typical active material loading of $\sim 1 \text{ mg cm}^{-2}$. Coin cells (CR2032 type) were assembled in an Ar-filled glovebox, using Li metal foil as counter/reference electrode, Celgard 2325 separator, and 1 M LiPF₆ in EC/DEC (1:1 v/v) as electrolyte

Table 3. 1 Electrode formulations

Electrode	NG:Si:SA ratio	Si type	Composition (slurry)		
			NG (mg)	Si (mg)	SA (mg)
NGE	9:0:1	-	252	0	28
PrSi-10/NGE	8:1:1	Pristine	224	28	28
PrSi-20/NGE	7:2:1	Pristine	196	56	28
PrSi-45/NGE	4.5:4.5:1	Pristine	126	126	28
PoSi-10/NGE	8:1:1	Porous (Si-220-HP)	224	28	28
PoSi-20/NGE	7:2:1	Porous (Si-220-HP)	196	56	28
PoSi-45/NGE	4.5:4.5:1	Porous (Si-220-HP)	126	126	28

3.3 Characterization techniques

Textural analysis: Surface area and pore size distribution were determined by N₂ adsorption-desorption (TriStar II Plus, Micromeritics), using the BET method for surface area and BJH for pore size distribution. Samples were degassed at 300 °C for 1 h prior to measurement.

Morphology and composition: SEM (TESCAN MAIA3 Triglav™) was used for imaging, with EDS for elemental mapping. PSD was measured via laser diffraction (Mastersizer 3000, Malvern) with wet dispersion.

Structural analysis: XRD (PANalytical X'Pert Powder, Cu K α , 2 θ = 10-80°) was used for phase identification, and Raman spectroscopy (Horiba XploRA PLUS, 532 nm excitation) probed bonding and crystallinity.

Surface chemistry: XPS (Kratos Axis Supra+, Al K α source) was conducted under ultrahigh vacuum, with high-resolution scans at 20 eV pass energy and survey scans at 80 eV. Binding energies were calibrated to O 1s at 532.8 eV.

Thermal stability: TGA (Netzsch STA 449 F1 Jupiter) was carried out from room temperature to 1100 °C under sequential N₂ and O₂ atmospheres to evaluate decomposition and oxidation behavior.

Electrochemical characterization: CV (0.01-1.5 V, 0.1 mV s⁻¹), galvanostatic charge-discharge cycling (0.01-1.5 V, 0.1C unless otherwise noted), rate capability tests, and EIS (0.1 Hz-100 kHz) were performed using a PARSTAT MC multichannel potentiostat/galvanostat (Ametek). Capacities were normalized to the mass of active material (Si + NG).

4 Results and Discussion

4.1 Development of porous silicon microparticles (Paper I)

The development of porous Si microparticles formed the first stage of this work. The goal was to establish a scalable, environmentally benign thermochemical route to induce porosity in metallurgical-grade Si, eliminating the need for HF while maintaining crystalline integrity. The approach relied on the decomposition of urea under controlled thermal and pressure conditions to trigger simultaneous chemical modification and mechanically assisted pore formation within the Si particles.

Upon heating above its melting point (~ 135 °C), urea is expected to infiltrate the voids between Si microparticles and gradually decompose, producing gaseous ammonia (NH_3), isocyanic acid (HNCO), and carbon dioxide (CO_2). These products play complementary roles: NH_3 and HNCO interact with the native surface oxides of Si, potentially forming unstable $-\text{Si}-\text{O}-\text{H}$ species that can be displaced by water molecules present during the treatment or later at post-treatment washing.¹⁵⁵ Meanwhile, the evolution of gases, especially within a confined environment, creates transient pressure gradients that mechanically disrupt the surface. Prior mechanistic studies have shown that partially decomposed urea and its intermediates (e.g., biuret, cyanuric acid) can form a viscous, foam-like melt that expands within confined spaces before solidifying.^{156,157} This expansion, coupled with chemical interaction at the gas-solid interface, is believed to contribute to the initiation of mesoporosity under relatively mild conditions. The structural transformation of pristine Si into mesoporous particles following urea-assisted treatment is

illustrated in Figure 4.1, combining SEM and nitrogen sorption analyses.

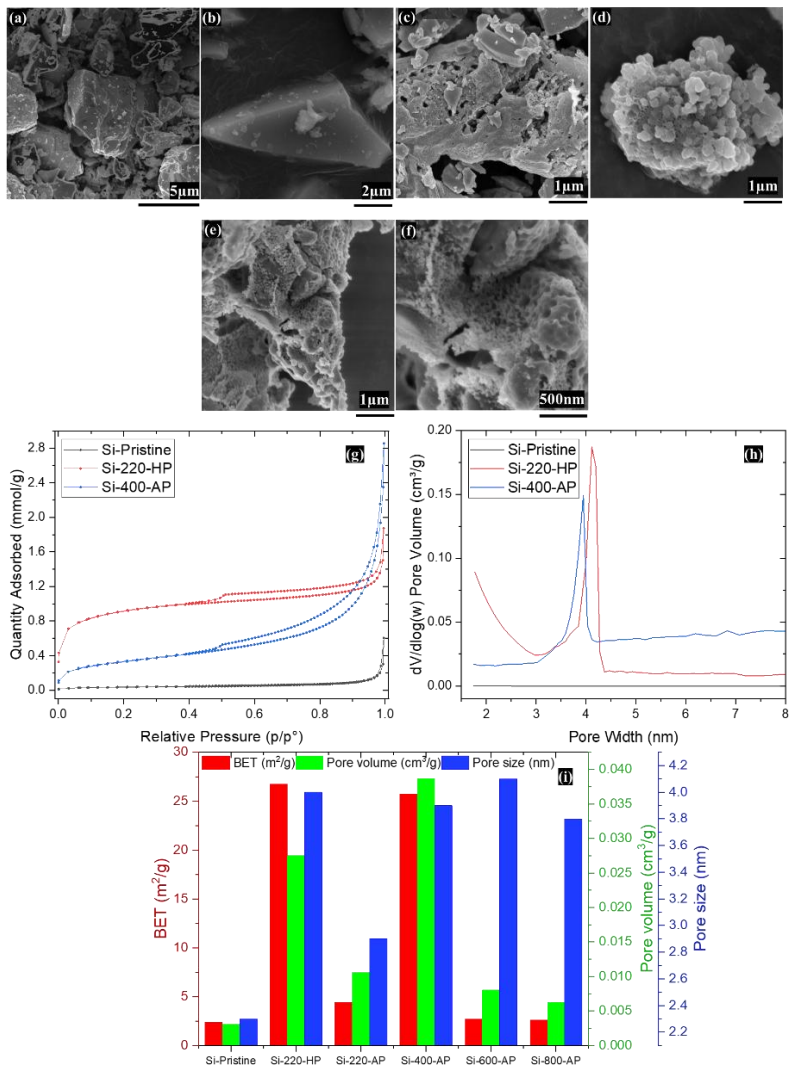


Figure 4. 1 Morphological and textural characteristics of pristine and urea-treated silicon microparticles. (a-b) Dense, non-porous pristine silicon (Si-Pristine). (c-d) Si-220-HP showing surface roughening and well-connected mesopores formed under confined conditions. (e-f) Si-400-AP exhibiting more open surface structures after atmospheric treatment. (g-h) Nitrogen adsorption-desorption isotherms and BJH pore size distributions confirming mesoporosity. (i) Comparison of BET surface area, pore volume, and average pore diameter as a function of treatment condition.

The untreated Si consisted of dense, angular microparticles ($\sim 4\text{-}5\ \mu\text{m}$) with smooth surfaces and negligible porosity, as confirmed by SEM and nitrogen sorption analyses (BET surface area $\approx 2.3\ \text{m}^2\ \text{g}^{-1}$, pore volume $\approx 0.003\ \text{cm}^3\ \text{g}^{-1}$).

Upon treatment, two samples stood out (Si-220-HP and Si-400-AP) both exhibiting pronounced surface restructuring and the development of mesoporosity. The Si-220-HP sample displayed roughened surfaces with well-connected mesopores ($\sim 4\ \text{nm}$) visible in SEM, consistent with its high measured surface area ($26.7\ \text{m}^2\ \text{g}^{-1}$) and pore volume ($0.028\ \text{cm}^3\ \text{g}^{-1}$). These features are attributed to confined urea decomposition gases that remain in contact with the Si surface, inducing localized mechanical stress and chemical etching. In contrast, Si-220-AP, treated under open conditions, exhibited only surface roughening and occasional microcracks in localized areas, which were not consistently observed for all particles in agreement with its lower BET surface area ($4.4\ \text{m}^2\ \text{g}^{-1}$). At elevated temperatures ($400\text{-}800\ \text{°C}$), the morphology evolved from fine to coarser textures. The Si-400-AP sample exhibited a visibly rougher surface with numerous interconnected pore openings and achieved the highest total pore volume ($0.039\ \text{cm}^3\ \text{g}^{-1}$), reflecting more extensive surface modification at this temperature. Further heating to $600\ \text{°C}$ and $800\ \text{°C}$ resulted in rapid urea decomposition and gas escape,^{156,158} producing primarily surface roughness rather than developed pore networks. Under these conditions, reactions appeared surface-limited and transient, preventing extended porosity formation.

Gravimetric analysis supported these textural observations: the highest etching yield (17.5 %) and rate ($14.6\ \text{mg}\ \text{h}^{-1}$) were measured for Si-400-AP, followed closely by Si-220-HP (15.2 %, $12.7\ \text{mg}\ \text{h}^{-1}$). The corresponding overall porosity was estimated at $\sim 6\text{-}8\ \%$, confirming

that moderate temperature and effective gas confinement are key factors in determining the extent of modification.¹⁵⁹⁻¹⁶¹

Elemental characterization further clarified the role of the reaction atmosphere. EDS analysis revealed an increase in surface oxygen from ~3 wt % in pristine Si to ~27 wt % in Si-220-HP and ~32 wt % in Si-400-AP. This trend correlates with increased surface area and indicates enhanced oxidation of newly exposed surfaces. Under confined conditions, decomposition gases (NH₃, H₂CO) and residual moisture may promote a dynamic cycle of surface oxidation and partial dissolution, leading to the formation of pores while altering the surface chemistry which will be seen later.¹⁶²⁻¹⁶⁴

X-ray diffraction (Figure 4. 2 a) confirmed that all treated samples retained the diamond-cubic Si structure (JCPDS 27-1402),¹⁶⁵ with only minor broadening of the (111) peak. The apparent crystallite size¹⁶⁶ decreased from ~55 nm in pristine Si to ~48 nm after treatment, indicating slight microstrain and lattice refinement without the formation of amorphous phases.^{167,168} Raman spectroscopy (Figure 4. 2 b) supported these findings: all samples displayed the characteristic first-order phonon near 520 cm⁻¹, with the treated materials showing a small redshift (to ≈ 518.6 cm⁻¹) and moderate peak broadening (FWHM ≈ 13-16 cm⁻¹). These features suggest the presence of local disorder and phonon confinement effects arising from nanostructuring and surface oxidation¹⁶⁹ rather than bulk structural collapse.¹⁷⁰⁻¹⁷²

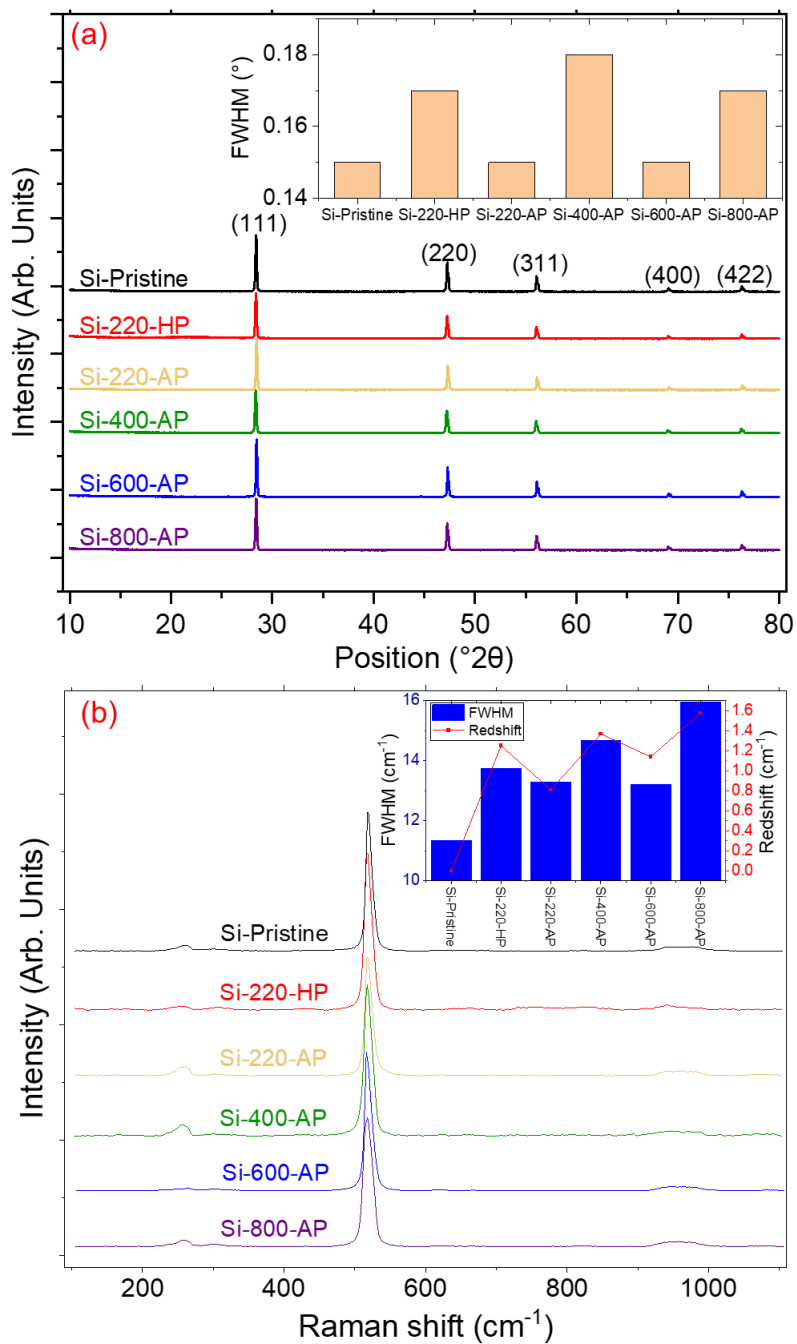


Figure 4. 2 XRD (a) and Raman analysis (b) confirming retained crystallinity and mild lattice disorder in urea-treated silicon microparticles.

X-ray photoelectron spectroscopy provided additional insight into surface chemistry (Figure 4. 3). The Si 2p spectra of treated samples were dominated by oxide-related peaks, while a new N 1s signal appeared between 398.5 and 402.5 eV. Deconvolution identified components associated with Si-N (~398.5 eV), amine ($-\text{NH}_2$, ~399.5 eV), protonated amine ($-\text{NH}_3^+$, ~401 eV), and oxidized nitrogen (NO_x , ~402.5 eV).¹⁷³⁻¹⁷⁵ These nitrogen species indicate partial incorporation of urea-derived intermediates and contribute to the formation of chemically enriched surfaces composed of mixed Si-O and Si-N functionalities. Complementary thermogravimetric analysis showed that the treated porous Si exhibited delayed oxidation onset (~900 °C, compared with ~650 °C for pristine Si), consistent with the presence of surface layers that limit oxygen diffusion and promote passivation (Paper 2).

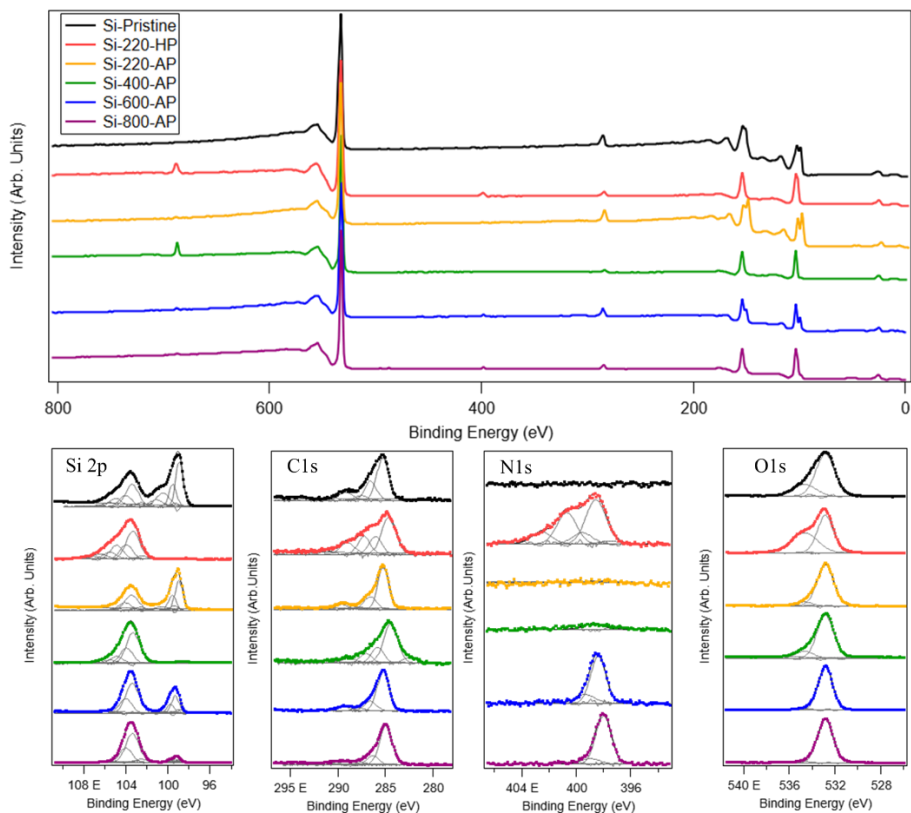


Figure 4. 3 XPS spectra showing surface chemistry changes in urea-treated silicon microparticles.

Overall, the urea-assisted thermochemical process appears to promote a combination of chemical etching and mechanical restructuring that generates mesoporosity while preserving crystallinity. Among the examined materials, Si-220-HP demonstrated the highest surface area, a balanced pore network, and chemically diverse surface states, whereas Si-400-AP achieved greater pore volume through extended gas-phase interaction. The Si-220-HP material was therefore selected for further investigation, as it offered a promising balance between porosity, surface modification, and potential passivation, making it a suitable candidate for integration into composite anodes discussed in the following section.

4.2 Integration of porous Si into graphite-based composite anodes (Paper II)

The electrochemical evaluation of the urea-derived porous Si (PoSi) focused on its integration within graphite-based composite electrodes and the resulting influence on performance compared to electrodes containing untreated pristine Si (PrSi). The objective was to assess whether the improved morphology and surface chemistry of PoSi, developed through the thermochemical route described in Section 4.1, translate into measurable electrochemical advantages when incorporated into LIB anodes.

This article includes studies on:

- Electrode Formation and Morphology
- Cyclic Voltammetry
- Electrochemical Impedance Spectroscopy (EIS)
- Cycling Stability and Rate Capability

The detailed results and discussion related to this article are not available in this version of the thesis, as the manuscript is currently under review for publication. The content will be made accessible once the publication has been approved.

5 Conclusions and Outlook

5.1 Main conclusions

This thesis establishes a green thermochemical route for modifying Si microparticles using urea as a benign etchant. Under confined conditions at moderate temperature, urea decomposition yields Si with well-connected surface mesopores while preserving the diamond-cubic crystal structure. The most distinctive textures were obtained for Si-220-HP (highest surface area, $\sim 26.7 \text{ m}^2 \text{ g}^{-1}$) and Si-400-AP (largest total pore volume, $\sim 0.039 \text{ cm}^3 \text{ g}^{-1}$), corresponding to an overall porosity on the order of 6-8%. XPS revealed the formation of Si–O and Si–N surface species, and thermogravimetry indicated delayed oxidation onset relative to pristine Si, consistent with partial passivation. Raman and XRD confirmed that the modifications are surface-confined and do not compromise bulk crystallinity.

When integrated into graphite-based composite anodes, the porous Si (Si-220-HP, PoSi) exhibited clear performance gains over pristine Si (PrSi) at equivalent loadings. Cyclic voltammetry showed sharper and more distinct Si redox features for PoSi composites after the initial formation cycle, while galvanostatic cycling demonstrated markedly improved capacity retention at moderate Si contents. After 100 cycles at 0.1 C, PoSi-10/NGE retained $\sim 636 \text{ mAh g}^{-1}$ from $\sim 701 \text{ mAh g}^{-1}$ initially ($\approx 90\%$ retention), and PoSi-20/NGE retained $\sim 888 \text{ mAh g}^{-1}$ from $\sim 1000 \text{ mAh g}^{-1}$ ($\approx 89\%$ retention), whereas corresponding PrSi composites declined toward graphite-level performance. Rate tests further showed 65-75 % capacity retention at 1 C and 60-70 % at 2 C relative to 0.1 C, with nearly full recovery upon returning to 0.1 C. This demonstrates that the porous Si structure and its interface with graphite remain mechanically and electrochemically stable under varying current loads. Although impedance measurements indicated

slightly higher charge-transfer resistance for PoSi, likely due to increased surface area and oxide coverage, this did not hinder long-term cycling stability.

Overall, the results confirm that urea-assisted thermochemical modification provides a scalable, HF-free route to mesostructured Si, where moderate porosity and tailored surface chemistry translate into tangible electrochemical improvements. At Si contents ≤ 20 wt %, the porous architecture offers partial mitigation of volume change, enhanced Li-ion transport, and chemically stable interfaces within the graphite matrix, leading to higher capacity and superior retention compared with pristine Si. These findings establish a solid foundation for future studies on stand-alone porous Si anodes and post-mortem analyses aimed at clarifying how porosity and surface chemistry govern lithium transport, stability, and long-term degradation.

5.2 Limitations of the study

Although this study successfully demonstrates a green, urea-assisted route for producing porous Si and its integration into graphite-based composite anodes, several limitations should be noted.

First, the synthesis and treatment steps were carried out on a laboratory scale. While the process is conceptually scalable and avoids hazardous chemicals, further work is needed to evaluate uniform heating, gas confinement, and reproducibility when scaled up.

Second, the characterization focused mainly on surface and structural features after treatment. The exact mechanisms that govern pore formation, particularly the roles of transient intermediates and gas-solid interactions, were not directly observed. Similarly, although Si–O and Si–N surface species were detected, their detailed spatial distribution and long-term stability under cycling remain to be clarified.

Electrochemical testing was limited to half-cell configurations with moderate Si loadings (≤ 20 wt%). The study did not include stand-alone porous Si anodes, full-cell systems, or long-term cycling beyond 100 cycles. As a result, the long-term degradation mechanisms and SEI evolution were not fully addressed.

Finally, the mechanical benefits of porosity were inferred from electrochemical behavior rather than measured directly. Additional in situ and post-mortem analyses will be required to confirm how porosity and surface chemistry influence structural stability during cycling.

5.3 Future work

The findings of this thesis provide a solid foundation for continued exploration of sustainable Si anodes, but several key directions remain open for future research.

- **Toward stand-alone porous silicon anodes**

Future work will focus on developing stand-alone porous Si anodes derived from the urea-assisted synthesis route. The promising results obtained from composite electrodes suggest that the moderate porosity and surface passivation achieved in this work could support stable electrochemical performance even without graphite buffering. To realize this, further optimization of particle morphology, porosity gradient, and surface composition will be necessary to balance ion accessibility with mechanical integrity.

Electrode engineering will also play a critical role, for example, exploring alternative binders and conductive matrices that can accommodate volume fluctuations while maintaining electronic connectivity. Moreover, full-cell configurations against commercial cathodes will be required to assess the practical energy density, coulombic efficiency, and compatibility of porous Si with industrially

relevant electrolytes. These studies will help bridge the gap between proof-of-concept composites and functional, stand-alone porous Si anodes suitable for next-generation lithium-ion batteries

- **Porosity and degradation mechanisms: an outlook**

Understanding how porosity and surface chemistry influence the long-term behavior of Si-based anodes remains a crucial step toward their practical deployment. Future studies should therefore include systematic post-mortem and in situ analyses to track structural and chemical evolution during cycling. Techniques such as focused ion beam-SEM, transmission electron microscopy, and X-ray tomography could be used to visualize pore collapse, crack propagation, and SEI growth in real time. Complementary spectroscopy (XPS, FTIR, NMR) may reveal how surface species such as Si–O and Si–N evolve under repeated lithiation-delithiation.

These analyses will clarify whether the moderate porosity introduced through the urea-assisted route primarily facilitates lithium transport, buffers mechanical stress, or contributes to surface passivation, and how these factors change with cycling and electrolyte interaction. A deeper mechanistic understanding of these degradation pathways will guide the design of optimized porous architectures and surface chemistries, improving both stability and capacity retention in future Si anode materials

6 Bibliography

- (1) *Energy Storage*; World Scientific Series in Current Energy Issues; World Scientific, 2017; Vol. Volume 4.
<https://doi.org/10.1142/10420>.
- (2) Muchuweni, E.; Mombeshora, E. T.; Muiva, C. M.; Sathiaraj, T. S. Lithium-Ion Batteries: Recent Progress in Improving the Cycling and Rate Performances of Transition Metal Oxide Anodes by Incorporating Graphene-Based Materials. *J. Energy Storage* **2023**, *73*, 109013.
<https://doi.org/10.1016/j.est.2023.109013>.
- (3) Placke, T.; Kloepsch, R.; Dühnen, S.; Winter, M. Lithium Ion, Lithium Metal, and Alternative Rechargeable Battery Technologies: The Odyssey for High Energy Density. *J. Solid State Electrochem.* **2017**, *21* (7), 1939–1964.
<https://doi.org/10.1007/s10008-017-3610-7>.
- (4) Zhang, H.; Wang, L.; Li, H.; He, X. Criterion for Identifying Anodes for Practically Accessible High-Energy-Density Lithium-Ion Batteries. *ACS Energy Lett.* **2021**, *6* (10), 3719–3724.
<https://doi.org/10.1021/acsenerylett.1c01713>.
- (5) Bai, S.; Bao, W.; Qian, K.; Han, B.; Li, W.; Sayahpour, B.; Sreenarayanan, B.; Tan, D. H. S.; Ham, S.; Meng, Y. S. Elucidating the Role of Prelithiation in Si-Based Anodes for Interface Stabilization. *Adv. Energy Mater.* **2023**, *13* (28), 2301041. <https://doi.org/10.1002/aenm.202301041>.
- (6) Liu, H.; Sun, Q.; Zhang, H.; Cheng, J.; Li, Y.; Zeng, Z.; Zhang, S.; Xu, X.; Ji, F.; Li, D.; Lu, J.; Ci, L. The Application Road of Silicon-Based Anode in Lithium-Ion Batteries: From Liquid Electrolyte to Solid-State Electrolyte. *Energy Storage Mater.* **2023**, *55*, 244–263. <https://doi.org/10.1016/j.ensm.2022.11.054>.
- (7) Liu, X.; Sun, X.; Shi, X.; Song, D.; Zhang, H.; Li, C.; Wang, K.-Y.; Xiao, C.; Liu, X.; Zhang, L. Low-Temperature and High-Performance Si/Graphite Composite Anodes Enabled by Sulfite Additive. *Chem. Eng. J.* **2021**, *421*, 127782.
<https://doi.org/10.1016/j.cej.2020.127782>.

- (8) Zhang, W.; Gui, S.; Li, W.; Tu, S.; Li, G.; Zhang, Y.; Sun, Y.; Xie, J.; Zhou, H.; Yang, H. Functionally Gradient Silicon/Graphite Composite Electrodes Enabling Stable Cycling and High Capacity for Lithium-Ion Batteries. *ACS Appl. Mater. Interfaces* **2022**, *14* (46), 51954–51964.
<https://doi.org/10.1021/acsami.2c15355>.
- (9) Jiang, M.; Chen, J.; Zhang, Y.; Song, N.; Jiang, W.; Yang, J. Assembly: A Key Enabler for the Construction of Superior Silicon-Based Anodes. *Adv. Sci.* **2022**, *9* (30), 2203162.
<https://doi.org/10.1002/advs.202203162>.
- (10) Sun, L.; Liu, Y.; Shao, R.; Wu, J.; Jiang, R.; Jin, Z. Recent Progress and Future Perspective on Practical Silicon Anode-Based Lithium Ion Batteries. *Energy Storage Mater.* **2022**, *46*, 482–502. <https://doi.org/10.1016/j.ensm.2022.01.042>.
- (11) Su, X.; Wu, Q.; Li, J.; Xiao, X.; Lott, A.; Lu, W.; Sheldon, B. W.; Wu, J. Silicon-Based Nanomaterials for Lithium-Ion Batteries: A Review. *Adv. Energy Mater.* **2014**, *4* (1), 1300882.
<https://doi.org/10.1002/aenm.201300882>.
- (12) Bitew, Z.; Tesemma, M.; Beyene, Y.; Amare, M. Nano-Structured Silicon and Silicon Based Composites as Anode Materials for Lithium Ion Batteries: Recent Progress and Perspectives. *Sustain. Energy Fuels* **2022**, *6* (4), 1014–1050.
<https://doi.org/10.1039/D1SE01494C>.
- (13) Zhang, F.; Zhu, W.; Li, T.; Yuan, Y.; Yin, J.; Jiang, J.; Yang, L. Advances of Synthesis Methods for Porous Silicon-Based Anode Materials. *Front. Chem.* **2022**, *10*.
<https://doi.org/10.3389/fchem.2022.889563>.
- (14) Ko, M.; Chae, S.; Cho, J. Challenges in Accommodating Volume Change of Si Anodes for Li-Ion Batteries. *ChemElectroChem* **2015**, *2* (11), 1645–1651.
<https://doi.org/10.1002/celec.201500254>.
- (15) Schwartz, B.; Robbins, H. Chemical Etching of Silicon: IV. Etching Technology. *J. Electrochem. Soc.* **1976**, *123* (12), 1903.
<https://doi.org/10.1149/1.2132721>.
- (16) Barillaro, G.; Nannini, A.; Piotta, M. Electrochemical Etching in HF Solution for Silicon Micromachining. *Sens. Actuators Phys.*

- 2002, 102 (1–2), 195–201. [https://doi.org/10.1016/S0924-4247\(02\)00385-0](https://doi.org/10.1016/S0924-4247(02)00385-0).
- (17) Knotter, D. M. Etching Mechanism of Vitreous Silicon Dioxide in HF-Based Solutions. *J. Am. Chem. Soc.* **2000**, 122 (18), 4345–4351. <https://doi.org/10.1021/ja993803z>.
- (18) Entwistle, J.; Rennie, A.; Patwardhan, S. A Review of Magnesiothermic Reduction of Silica to Porous Silicon for Lithium-Ion Battery Applications and Beyond. *J Mater Chem A* **2018**, 6 (38), 18344–18356. <https://doi.org/10.1039/C8TA06370B>.
- (19) Nijdam, A. J.; Van Suchtelen, J.; Berenschot, J. W.; Gardeniers, J. G.; Elwenspoek, M. Etching of Silicon in Alkaline Solutions: A Critical Look at the {1 1 1} Minimum. *J. Cryst. Growth* **1999**, 198, 430–434. [https://doi.org/10.1016/S0022-0248\(98\)01032-X](https://doi.org/10.1016/S0022-0248(98)01032-X).
- (20) Elwenspoek, M. On the Mechanism of Anisotropic Etching of Silicon. *J. Electrochem. Soc.* **1993**, 140 (7), 2075. <https://doi.org/10.1149/1.2220767>.
- (21) Saverina, E. A.; Zinchenko, D. Y.; Farafonova, S. D.; Galushko, A. S.; Novikov, A. A.; Gorbachevskii, M. V.; Ananikov, V. P.; Egorov, M. P.; Jouikov, V. V.; Syroeshkin, M. A. Porous Silicon Preparation by Electrochemical Etching in Ionic Liquids. *ACS Sustain. Chem. Eng.* **2020**, 8 (27), 10259–10264. <https://doi.org/10.1021/acssuschemeng.0c03133>.
- (22) Brack, W.; Heine, B.; Birkhold, F.; Kruse, M.; Schoch, G.; Tischer, S.; Deutschmann, O. Kinetic Modeling of Urea Decomposition Based on Systematic Thermogravimetric Analyses of Urea and Its Most Important By-Products. *Chem. Eng. Sci.* **2014**, 106, 1–8. <https://doi.org/10.1016/j.ces.2013.11.013>.
- (23) Schaber, P. M.; Colson, J.; Higgins, S.; Thielen, D.; Anspach, B.; Brauer, J. Thermal Decomposition (Pyrolysis) of Urea in an Open Reaction Vessel. *Thermochim. Acta* **2004**, 424 (1), 131–142. <https://doi.org/10.1016/j.tca.2004.05.018>.
- (24) Honorien, J.; Fournet, R.; Glaude, P.-A.; Sirjean, B. Theoretical Study of the Gas-Phase Thermal Decomposition of Urea. *Proc. Combust. Inst.* **2021**, 38 (1), 355–364. <https://doi.org/10.1016/j.proci.2020.06.012>.

- (25) Chen, L.-C.; Chen, M.; Tsauro, T.-H.; Lien, C.; Wan, C.-C. Selective Etching of Silicon in Aqueous Ammonia Solution. *Sens. Actuators Phys.* **1995**, *49* (1), 115–121. [https://doi.org/10.1016/0924-4247\(95\)01007-N](https://doi.org/10.1016/0924-4247(95)01007-N).
- (26) Fichtner, M.; Edström, K.; Ayerbe, E.; Berecibar, M.; Bhowmik, A.; Castelli, I. E.; Clark, S.; Dominko, R.; Erakca, M.; Franco, A. A.; Grimaud, A.; Horstmann, B.; Latz, A.; Lorrmann, H.; Meeus, M.; Narayan, R.; Pammer, F.; Ruhland, J.; Stein, H.; Vegge, T.; Weil, M. Rechargeable Batteries of the Future—The State of the Art from a BATTERY 2030+ Perspective. *Adv. Energy Mater.* **2022**, *12* (17), 2102904. <https://doi.org/10.1002/aenm.202102904>.
- (27) Brodd, R. J. Synopsis of the Lithium-Ion Battery Markets. In *Lithium-Ion Batteries: Science and Technologies*; Yoshio, M., Brodd, R. J., Kozawa, A., Eds.; Springer New York: New York, NY, 2009; pp 1–7. https://doi.org/10.1007/978-0-387-34445-4_1.
- (28) Deng, C.; Li, X.; Chen, R.; Ye, K.; Lipton, J.; Maclean, S. A.; Wang, H.; Taylor, A. D.; Weng, G. M. Recent Advances in Rocking Chair Batteries and Beyond. *Energy Storage Mater.* **2023**, *60*, 102820. <https://doi.org/10.1016/j.ensm.2023.102820>.
- (29) R. Jacob Robin. Viability and Eco-Consequences of Synthetic and Natural Graphite for Lithium-Ion Battery Anodes in the USA. *IEEE Eng. Manag. Rev.* **2024**, *52* (3), 131–147. <https://doi.org/10.1109/EMR.2024.3372697>.
- (30) Yi, X.; Qi, G.; Liu, X.; Depcik, C.; Liu, L. Challenges and Strategies toward Anode Materials with Different Lithium Storage Mechanisms for Rechargeable Lithium Batteries. *J. Energy Storage* **2024**, *95*, 112480. <https://doi.org/10.1016/j.est.2024.112480>.
- (31) Usai, L.; Lamb, J. J.; Hertwich, E.; Burheim, O. S.; Strømman, A. H. Analysis of the Li-Ion Battery Industry in Light of the Global Transition to Electric Passenger Light Duty Vehicles until 2050. *Environ. Res. Infrastruct. Sustain.* **2022**, *2* (1), 011002. <https://doi.org/10.1088/2634-4505/ac49a0>.
- (32) Łukasz, B.; Rybakowska, I.; Krakowiak, A.; Gregorczyk, M.; Waldman, W. Lithium Batteries Safety, Wider Perspective. *Int J*

- Occup Med Env. Health* **2023**, 36 (1), 3–20.
<https://doi.org/10.13075/ijomeh.1896.01995>.
- (33) Muralidharan, N.; Self, E. C.; Nanda, J.; Belharouak, I. Next-Generation Cobalt-Free Cathodes – A Prospective Solution to the Battery Industry’s Cobalt Problem*. In *Transition Metal Oxides for Electrochemical Energy Storage*; 2022; pp 33–53.
<https://doi.org/10.1002/9783527817252.ch3>.
- (34) Bouguern, M. D.; M R, A. K.; Zaghbi, K. The Critical Role of Interfaces in Advanced Li-Ion Battery Technology: A Comprehensive Review. *J. Power Sources* **2024**, 623, 235457.
<https://doi.org/10.1016/j.jpowsour.2024.235457>.
- (35) Cheng, H.; Shapter, J. G.; Li, Y.; Gao, G. Recent Progress of Advanced Anode Materials of Lithium-Ion Batteries. *J. Energy Chem.* **2021**, 57, 451–468.
<https://doi.org/10.1016/j.jechem.2020.08.056>.
- (36) Wang, K.; Xu, Y.; Wu, H.; Yuan, R.; Zong, M.; Li, Y.; Dravid, V.; Ai, W.; Wu, J. A Hybrid Lithium Storage Mechanism of Hard Carbon Enhances Its Performance as Anodes for Lithium-Ion Batteries. *Carbon* **2021**, 178, 443–450.
<https://doi.org/10.1016/j.carbon.2020.11.095>.
- (37) Ogumi, Z.; Wang, H. Carbon Anode Materials. In *Lithium-Ion Batteries: Science and Technologies*; Yoshio, M., Brodd, R. J., Kozawa, A., Eds.; Springer New York: New York, NY, 2009; pp 49–73. https://doi.org/10.1007/978-0-387-34445-4_3.
- (38) Xue, Z.; Wang, Z.; Zhang, J.; Lu, Y.; Huang, W.; Chen, A.; Zhao, C.; Elena, K.; Elena, K.; Vladimir, K.; Fan, L.; Zhang, Q. The Role, Formation and Characterization of LiC₆ in Composite Lithium Anodes. *New Carbon Mater.* **2023**, 38 (4), 641–655.
[https://doi.org/10.1016/S1872-5805\(23\)60773-5](https://doi.org/10.1016/S1872-5805(23)60773-5).
- (39) Lin, X.; Khosravinia, K.; Hu, X.; Li, J.; Lu, W. Lithium Plating Mechanism, Detection, and Mitigation in Lithium-Ion Batteries. *Prog. Energy Combust. Sci.* **2021**, 87, 100953.
<https://doi.org/10.1016/j.pecs.2021.100953>.
- (40) Singh, J.; Zhu, Z.; Han, S.; Wang, N.; Tiwari, S. K. Advances in Hard Carbon: From Structural Complexity to Applications for

- next-Generation Technologies. *J. Alloys Compd.* **2025**, *1042*, 183755. <https://doi.org/10.1016/j.jallcom.2025.183755>.
- (41) Xie, L.; Tang, C.; Bi, Z.; Song, M.; Fan, Y.; Yan, C.; Li, X.; Su, F.; Zhang, Q.; Chen, C. Hard Carbon Anodes for Next-Generation Li-Ion Batteries: Review and Perspective. *Adv. Energy Mater.* **2021**, *11* (38), 2101650. <https://doi.org/10.1002/aenm.202101650>.
- (42) Babu, B.; Simon, P.; Balducci, A. Fast Charging Materials for High Power Applications. *Adv. Energy Mater.* **2020**, *10* (29), 2001128. <https://doi.org/10.1002/aenm.202001128>.
- (43) Yan, H.; Zhang, D.; Qilu; Duo, X.; Sheng, X. A Review of Spinel Lithium Titanate (Li₄Ti₅O₁₂) as Electrode Material for Advanced Energy Storage Devices. *Ceram. Int.* **2021**, *47* (5), 5870–5895. <https://doi.org/10.1016/j.ceramint.2020.10.241>.
- (44) Li, X.; Zhang, J.; An, X.; Liu, Q.; Xie, L.; Yao, W.; Kong, Q. Crystal Structure Regulation of Trititanium Pentoxide for Advanced Zero-Strain Lithium Storage Anode. *J. Colloid Interface Sci.* **2025**, *678*, 566–574. <https://doi.org/10.1016/j.jcis.2024.09.138>.
- (45) Dimov, N. Development of Metal Alloy Anodes. In *Lithium-Ion Batteries: Science and Technologies*; Yoshio, M., Brodd, R. J., Kozawa, A., Eds.; Springer New York: New York, NY, 2009; pp 241–265. https://doi.org/10.1007/978-0-387-34445-4_11.
- (46) Shang, Y.; Li, H.; Ma, T.; Yang, Y.; Jiang, Y.; Yu, W. Suppression Strategies for Si Anode Volume Expansion in Li-Ion Batteries Based on Structure Design and Modification: A Review. *ACS Appl. Mater. Interfaces* **2025**, *17* (22), 31730–31753. <https://doi.org/10.1021/acsami.5c00948>.
- (47) Lu, Y.; Yu, L.; Lou, X. W. (David). Nanostructured Conversion-Type Anode Materials for Advanced Lithium-Ion Batteries. *Chem* **2018**, *4* (5), 972–996. <https://doi.org/10.1016/j.chempr.2018.01.003>.
- (48) Wei, X.; Wang, X.; Tan, X.; An, Q.; Mai, L. Nanostructured Conversion-Type Negative Electrode Materials for Low-Cost and High-Performance Sodium-Ion Batteries. *Adv. Funct. Mater.* **2018**, *28* (46), 1804458. <https://doi.org/10.1002/adfm.201804458>.

- (49) Saidi, N. M.; Abdah, M. A. A. M.; Mustafa, M. N.; Walvekar, R.; Khalid, M.; Khosla, A. Advancements in Silicon Anodes for Enhanced Lithium-Ion Batteries Performance: Innovations Toward Next-Gen Superbatteries. *Battery Energy* **2025**, *4* (5), e20240048. <https://doi.org/10.1002/bte2.20240048>.
- (50) Tao, J.; Liu, L.; Han, J.; Peng, J.; Chen, Y.; Yang, Y.; Yao, H.; Li, J.; Huang, Z.; Lin, Y. New Perspectives on Spatial Dynamics of Lithiation and Lithium Plating in Graphite/Silicon Composite Anodes. *Energy Storage Mater.* **2023**, *60*, 102809. <https://doi.org/10.1016/j.ensm.2023.102809>.
- (51) Grey, C. P.; Tarascon, J. M. Sustainability and in Situ Monitoring in Battery Development. *Nat. Mater.* **2017**, *16* (1), 45–56. <https://doi.org/10.1038/nmat4777>.
- (52) Taylor, S. R.; McLennan, S. M. The Geochemical Evolution of the Continental Crust. *Rev. Geophys.* **1995**, *33* (2), 241–265. <https://doi.org/10.1029/95RG00262>.
- (53) Larcher, D.; Mudalige, C.; George, A. E.; Porter, V.; Gharghouri, M.; Dahn, J. R. Si-Containing Disordered Carbons Prepared by Pyrolysis of Pitch/Polysilane Blends: Effect of Oxygen and Sulfur. *Solid State Ion.* **1999**, *122* (1), 71–83. [https://doi.org/10.1016/S0167-2738\(98\)00557-8](https://doi.org/10.1016/S0167-2738(98)00557-8).
- (54) Sharma, R. A.; Seefurth, R. N. Thermodynamic Properties of the Lithium-Silicon System. *J. Electrochem. Soc.* **1976**, *123* (12), 1763. <https://doi.org/10.1149/1.2132692>.
- (55) Park, C.-M.; Kim, J.-H.; Kim, H.; Sohn, H.-J. Li-Alloy Based Anode Materials for Li Secondary Batteries. *Chem. Soc. Rev.* **2010**, *39* (8), 3115–3141. <https://doi.org/10.1039/B919877F>.
- (56) Li, J.-Y.; Xu, Q.; Li, G.; Yin, Y.-X.; Wan, L.-J.; Guo, Y.-G. Research Progress Regarding Si-Based Anode Materials towards Practical Application in High Energy Density Li-Ion Batteries. *Mater. Chem. Front.* **2017**, *1* (9), 1691–1708. <https://doi.org/10.1039/C6QM00302H>.
- (57) Ashuri, M.; He, Q.; Shaw, L. L. Silicon as a Potential Anode Material for Li-Ion Batteries: Where Size, Geometry and Structure Matter. *Nanoscale* **2016**, *8* (1), 74–103. <https://doi.org/10.1039/C5NR05116A>.

- (58) Zhu, B.; Liu, G.; Lv, G.; Mu, Y.; Zhao, Y.; Wang, Y.; Li, X.; Yao, P.; Deng, Y.; Cui, Y.; Zhu, J. Minimized Lithium Trapping by Isovalent Isomorphism for High Initial Coulombic Efficiency of Silicon Anodes. *Sci. Adv.* **5** (11), eaax0651. <https://doi.org/10.1126/sciadv.aax0651>.
- (59) Shin, J.; Kim, T.-H.; Lee, Y.; Cho, E. Key Functional Groups Defining the Formation of Si Anode Solid-Electrolyte Interphase towards High Energy Density Li-Ion Batteries. *Energy Storage Mater.* **2020**, *25*, 764–781. <https://doi.org/10.1016/j.ensm.2019.09.009>.
- (60) Rehnlund, D.; Lindgren, F.; Böhme, S.; Nordh, T.; Zou, Y.; Pettersson, J.; Bexell, U.; Boman, M.; Edström, K.; Nyholm, L. Lithium Trapping in Alloy Forming Electrodes and Current Collectors for Lithium Based Batteries. *Energy Environ. Sci.* **2017**, *10* (6), 1350–1357. <https://doi.org/10.1039/C7EE00244K>.
- (61) Ge, M.; Fang, X.; Rong, J.; Zhou, C. Review of Porous Silicon Preparation and Its Application for Lithium-Ion Battery Anodes. *Nanotechnology* **2013**, *24* (42), 422001. <https://doi.org/10.1088/0957-4484/24/42/422001>.
- (62) Wu, H.; Cui, Y. Designing Nanostructured Si Anodes for High Energy Lithium Ion Batteries. *Nano Today* **2012**, *7* (5), 414–429. <https://doi.org/10.1016/j.nantod.2012.08.004>.
- (63) Li, L.; Deng, Y.; Hu, K.; Xu, B.; Wang, N.; Bai, Z.; Xu, X.; Yang, J. Nanostructure Designing and Hybridizing of High-Capacity Silicon-Based Anode for Lithium-Ion Batteries. *Prog. Nat. Sci. Mater. Int.* **2023**, *33* (1), 16–36. <https://doi.org/10.1016/j.pnsc.2023.02.001>.
- (64) Zhang, Z.; Ma, R.; Yang, J.; Wang, J.; Peng, Y. A Review on Mechanical, Electrical, Chemical, and Electrochemical Properties of Coating Materials for Silicon Anodes in Lithium-Ion Batteries. *Small* **2025**, *21* (39), e06400. <https://doi.org/10.1002/smll.202506400>.
- (65) Kennedy, T.; Brandon, M.; Ryan, K. M. Advances in the Application of Silicon and Germanium Nanowires for High-Performance Lithium-Ion Batteries. *Adv. Mater.* **2016**, *28* (27), 5696–5704. <https://doi.org/10.1002/adma.201503978>.

- (66) Yu, R.; Pan, Y.; Jiang, Y.; Zhou, L.; Zhao, D.; Van Tendeloo, G.; Wu, J.; Mai, L. Regulating Lithium Transfer Pathway to Avoid Capacity Fading of Nano Si Through Sub-Nano Scale Interfused SiO_x/C Coating. *Adv. Mater.* **2023**, *35* (49), 2306504. <https://doi.org/10.1002/adma.202306504>.
- (67) Choi, S.; Jung, D. S.; Choi, J. W. Scalable Fracture-Free SiOC Glass Coating for Robust Silicon Nanoparticle Anodes in Lithium Secondary Batteries. *Nano Lett.* **2014**, *14* (12), 7120–7125. <https://doi.org/10.1021/nl503620z>.
- (68) Gu, M.; Li, Y.; Li, X.; Hu, S.; Zhang, X.; Xu, W.; Thevuthasan, S.; Baer, D. R.; Zhang, J.-G.; Liu, J.; Wang, C. In Situ TEM Study of Lithiation Behavior of Silicon Nanoparticles Attached to and Embedded in a Carbon Matrix. *ACS Nano* **2012**, *6* (9), 8439–8447. <https://doi.org/10.1021/nn303312m>.
- (69) McDowell, M. T.; Lee, S. W.; Harris, J. T.; Korgel, B. A.; Wang, C.; Nix, W. D.; Cui, Y. In Situ TEM of Two-Phase Lithiation of Amorphous Silicon Nanospheres. *Nano Lett.* **2013**, *13* (2), 758–764. <https://doi.org/10.1021/nl3044508>.
- (70) Liu, X. H.; Zhong, L.; Huang, S.; Mao, S. X.; Zhu, T.; Huang, J. Y. Size-Dependent Fracture of Silicon Nanoparticles During Lithiation. *ACS Nano* **2012**, *6* (2), 1522–1531. <https://doi.org/10.1021/nn204476h>.
- (71) Zhang, L.; Wang, C.; Dou, Y.; Cheng, N.; Cui, D.; Du, Y.; Liu, P.; Al-Mamun, M.; Zhang, S.; Zhao, H. A Yolk–Shell Structured Silicon Anode with Superior Conductivity and High Tap Density for Full Lithium-Ion Batteries. *Angew. Chem. Int. Ed.* **2019**, *58* (26), 8824–8828. <https://doi.org/10.1002/anie.201903709>.
- (72) Yao, Y.; Rui, X.; Bai, R.; Ouyang, Y.; Li, G.; Zhao, Y.; Zhu, Y.-H.; Zhao, M.; Li, B.-Q.; Zhang, X.; Li, Z.; Ling, F.; Ma, C.; Ma, J.; Zhou, F.; Ren, Z.; Shi, X.; Zhao, Z.; Lu, Y.; Jia, B.-E.; Wu, N.; Wang, Z.; Yao, W.; Bi, S.; Chen, K.; Li, J.-Y.; Wu, J.-Y.; Li, J.-X.; Tu, W.-B.; Guan, J.; Wu, X.-L.; Zhang, X.-D.; Wang, K.; Ma, Y.; Zhu, C.; Wan, F.; Xie, D.; Lu, B.; Xu, J.-J.; Li, C.; Niu, Z.; Tang, Y.; Yan, Q.; Wen, Z.; Zhang, C.; Li, X.; Wu, Z.-S.; Huang, J.-Q.; Zhang, Q.; Xin, S.; Guo, Y.-G.; Yu, Y. Roadmap for Next-Generation Electrochemical Energy Storage Technologies:

- Secondary Batteries and Supercapacitors. *ACS Nano* **2025**, *19* (34), 30568–30687. <https://doi.org/10.1021/acsnano.4c10091>.
- (73) Aggarwal, P.; Umar, F.; Paul, A. Review of Ordered Pores in Nanomaterials for Energy Applications Ranging from Energy Storage to Catalysis. *ACS Appl. Nano Mater.* **2025**, *8* (37), 17780–17818. <https://doi.org/10.1021/acsanm.5c03047>.
- (74) He, J.; Deng, Y.; Han, J.; Xu, T.; Qi, J.; Li, J.; Zhang, Y.; Zhao, Z.; Li, Q.; Xiao, J.; Zhang, J.; Kong, D.; Wei, W.; Wu, S.; Yang, Q.-H. Sieving Pore Design Enables Stable and Fast Alloying Chemistry of Silicon Negative Electrodes in Li-Ion Batteries. *Nat. Commun.* **2025**, *16* (1), 4858. <https://doi.org/10.1038/s41467-025-60191-9>.
- (75) Shi, H.; Zhang, W.; Wang, J.; Wang, D.; Wang, C.; Xiong, Z.; Wu, J.; Bai, Z.; Yan, X. Scalable Synthesis of a Porous Structure Silicon/Carbon Composite Decorated with Copper as an Anode for Lithium Ion Batteries. *Appl. Surf. Sci.* **2023**, *620*, 156843. <https://doi.org/10.1016/j.apsusc.2023.156843>.
- (76) Shen, X.; Tian, Z.; Fan, R.; Shao, L.; Zhang, D.; Cao, G.; Kou, L.; Bai, Y. Research Progress on Silicon/Carbon Composite Anode Materials for Lithium-Ion Battery. *J. Energy Chem.* **2018**, *27* (4), 1067–1090. <https://doi.org/10.1016/j.jechem.2017.12.012>.
- (77) Suh, S.; Choi, H.; Eom, K.; Kim, H.-J. Enhancing the Electrochemical Properties of a Si Anode by Introducing Cobalt Metal as a Conductive Buffer for Lithium-Ion Batteries. *J. Alloys Compd.* **2020**, *827*, 154102. <https://doi.org/10.1016/j.jallcom.2020.154102>.
- (78) Feyzi, E.; M R, A. K.; Li, X.; Deng, S.; Nanda, J.; Zaghbi, K. A Comprehensive Review of Silicon Anodes for High-Energy Lithium-Ion Batteries: Challenges, Latest Developments, and Perspectives. *Energy* **2024**, *5*, 100176. <https://doi.org/10.1016/j.nxener.2024.100176>.
- (79) Yang, G.; Frisco, S.; Tao, R.; Philip, N.; Bennett, T. H.; Stetson, C.; Zhang, J.-G.; Han, S.-D.; Teeter, G.; Harvey, S. P.; Zhang, Y.; Veith, G. M.; Nanda, J. Robust Solid/Electrolyte Interphase (SEI) Formation on Si Anodes Using Glyme-Based Electrolytes.

- ACS Energy Lett.* **2021**, 6 (5), 1684–1693.
<https://doi.org/10.1021/acsenergylett.0c02629>.
- (80) Chen, J.; Fan, X.; Li, Q.; Yang, H.; Khoshi, M. R.; Xu, Y.; Hwang, S.; Chen, L.; Ji, X.; Yang, C.; He, H.; Wang, C.; Garfunkel, E.; Su, D.; Borodin, O.; Wang, C. Electrolyte Design for LiF-Rich Solid–Electrolyte Interfaces to Enable High-Performance Microsized Alloy Anodes for Batteries. *Nat. Energy* **2020**, 5 (5), 386–397. <https://doi.org/10.1038/s41560-020-0601-1>.
- (81) Lee, H.; Kim, A.; Kim, H.-S.; Jeon, C.-W.; Yoon, T. Inhibition of Si Fracture Via Rigid Solid Electrolyte Interphase in Lithium-Ion Batteries. *Adv. Energy Mater.* **2023**, 13 (5), 2202780. <https://doi.org/10.1002/aenm.202202780>.
- (82) Zhang, X.-Q.; Cheng, X.-B.; Chen, X.; Yan, C.; Zhang, Q. Fluoroethylene Carbonate Additives to Render Uniform Li Deposits in Lithium Metal Batteries. *Adv. Funct. Mater.* **2017**, 27 (10), 1605989. <https://doi.org/10.1002/adfm.201605989>.
- (83) Schiele, A.; Breitung, B.; Hatsukade, T.; Berkes, B. B.; Hartmann, P.; Janek, J.; Brezesinski, T. The Critical Role of Fluoroethylene Carbonate in the Gassing of Silicon Anodes for Lithium-Ion Batteries. *ACS Energy Lett.* **2017**, 2 (10), 2228–2233. <https://doi.org/10.1021/acsenergylett.7b00619>.
- (84) Olson, J. Z.; Johansson, P. K.; Castner, D. G.; Schlenker, C. W. Operando Sum-Frequency Generation Detection of Electrolyte Redox Products at Active Si Nanoparticle Li-Ion Battery Interfaces. *Chem. Mater.* **2018**, 30 (4), 1239–1248. <https://doi.org/10.1021/acs.chemmater.7b04087>.
- (85) Zhao, L.; Zhang, D.; Huang, Y.; Lin, K.; Chen, L.; Lv, W.; He, Y.-B.; Kang, F. Constructing a Reinforced and Gradient Solid Electrolyte Interphase on Si Nanoparticles by In-Situ Thiol-Ene Click Reaction for Long Cycling Lithium-Ion Batteries. *Small* **2021**, 17 (40), 2102316. <https://doi.org/10.1002/smll.202102316>.
- (86) Grill, J.; Popovic-Neuber, J. Long Term Porosity of Solid Electrolyte Interphase on Model Silicon Anodes with Liquid Battery Electrolytes. *Commun. Chem.* **2024**, 7 (1), 297. <https://doi.org/10.1038/s42004-024-01381-2>.

- (87) Wang, A.; Kadam, S.; Li, H.; Shi, S.; Qi, Y. Review on Modeling of the Anode Solid Electrolyte Interphase (SEI) for Lithium-Ion Batteries. *Npj Comput. Mater.* **2018**, *4* (1), 15. <https://doi.org/10.1038/s41524-018-0064-0>.
- (88) He, W.; Xu, W.; Li, Z.; Hu, Z.; Yang, J.; Qin, G.; Teng, W.; Zhang, T.; Zhang, W.; Sun, Z.; Yu, X. Structural Design and Challenges of Micron-Scale Silicon-Based Lithium-Ion Batteries. *Adv. Sci.* **2025**, *12* (6), 2407540. <https://doi.org/10.1002/advs.202407540>.
- (89) Hu, K.; Sang, X.; Chen, J.; Liu, Z.; Zhang, J.; Hu, X. High-Safety Lithium-Ion Batteries with Silicon-Based Anodes Enabled by Electrolyte Design. *Chem. – Asian J.* **2023**, *18* (24), e202300820. <https://doi.org/10.1002/asia.202300820>.
- (90) Lee, K. T.; Cho, J. Roles of Nanosize in Lithium Reactive Nanomaterials for Lithium Ion Batteries. *Nano Today* **2011**, *6* (1), 28–41. <https://doi.org/10.1016/j.nantod.2010.11.002>.
- (91) Yue, X.-Y.; Yao, Y.-X.; Zhang, J.; Li, Z.; Yang, S.-Y.; Li, X.-L.; Yan, C.; Zhang, Q. The Raw Mixed Conducting Interphase Affords Effective Prelithiation in Working Batteries. *Angew. Chem. Int. Ed.* **2022**, *61* (29), e202205697. <https://doi.org/10.1002/anie.202205697>.
- (92) Lin, S.; Li, X.; Zhang, J.; Guo, L.; Xu, X.; Yuan, W.; Liu, H.; Li, A.; Chen, X.; Song, H. Solid-State Amorphization to Alleviate Severe Volume Expansion in Silicon-Based Anodes. *J. Colloid Interface Sci.* **2025**, *699*, 138302. <https://doi.org/10.1016/j.jcis.2025.138302>.
- (93) Chen, X.; Cheng, W.; Liu, H.; Chen, H.; Ma, J.; Zhang, Y.; Wu, Z.; Wang, C.; You, Y.; Xing, X.; Wu, Z. Research Progresses on Nano-Structured Silicon-Based Materials as Anode for Lithium-Ion Batteries. *Materials* **2025**, *18* (4). <https://doi.org/10.3390/ma18040830>.
- (94) An, W.; Gao, B.; Mei, S.; Xiang, B.; Fu, J.; Wang, L.; Zhang, Q.; Chu, P. K.; Huo, K. Scalable Synthesis of Ant-Nest-like Bulk Porous Silicon for High-Performance Lithium-Ion Battery Anodes. *Nat. Commun.* **2019**, *10* (1), 1447. <https://doi.org/10.1038/s41467-019-09510-5>.

- (95) Sim, S.; Oh, P.; Park, S.; Cho, J. Critical Thickness of SiO₂ Coating Layer on Core@Shell Bulk@Nanowire Si Anode Materials for Li-Ion Batteries. *Adv. Mater.* **2013**, *25* (32), 4498–4503. <https://doi.org/10.1002/adma.201301454>.
- (96) He, Y.; Yu, X.; Wang, Y.; Li, H.; Huang, X. Alumina-Coated Patterned Amorphous Silicon as the Anode for a Lithium-Ion Battery with High Coulombic Efficiency. *Adv. Mater.* **2011**, *23* (42), 4938–4941. <https://doi.org/10.1002/adma.201102568>.
- (97) Li, J.; Xiao, X.; Cheng, Y.-T.; Verbrugge, M. W. Atomic Layered Coating Enabling Ultrafast Surface Kinetics at Silicon Electrodes in Lithium Ion Batteries. *J. Phys. Chem. Lett.* **2013**, *4* (20), 3387–3391. <https://doi.org/10.1021/jz4018255>.
- (98) Zhang, Y.; Qin, X.; Liu, Y.; Lei, C.; Wei, T.; Guo, Z. Double-Shell-Structured Si@Al₂O₃@C Nanoparticles as High-Performance Anode Materials for Lithium-Ion Batteries. *J. Alloys Compd.* **2022**, *923*, 166428. <https://doi.org/10.1016/j.jallcom.2022.166428>.
- (99) Xiao, X.; Lu, P.; Ahn, D. Ultrathin Multifunctional Oxide Coatings for Lithium Ion Batteries. *Adv. Mater.* **2011**, *23* (34), 3911–3915. <https://doi.org/10.1002/adma.201101915>.
- (100) Zhu, H.; Shiraz, M. H. A.; Liu, L.; Hu, Y.; Liu, J. A Facile and Low-Cost Al₂O₃ Coating as an Artificial Solid Electrolyte Interphase Layer on Graphite/Silicon Composites for Lithium-Ion Batteries. *Nanotechnology* **2021**, *32* (14), 144001. <https://doi.org/10.1088/1361-6528/abd580>.
- (101) Casino, S.; Heidrich, B.; Makvandi, A.; Beuse, T.; Gallasch, T.; Peterlechner, M.; Wilde, G.; Winter, M.; Niehoff, P. Al₂O₃ Protective Coating on Silicon Thin Film Electrodes and Its Effect on the Aging Mechanisms of Lithium Metal and Lithium Ion Cells. *J. Energy Storage* **2021**, *44*, 103479. <https://doi.org/10.1016/j.est.2021.103479>.
- (102) Shin, J.; Cho, E. Agglomeration Mechanism and a Protective Role of Al₂O₃ for Prolonged Cycle Life of Si Anode in Lithium-Ion Batteries. *Chem. Mater.* **2018**, *30* (10), 3233–3243. <https://doi.org/10.1021/acs.chemmater.8b00145>.

- (103) Zhang, Q.; Han, L.; Pan, J.; Chen, Z.; Cheng, Y.-T. Chemically Stable Artificial SEI for Li-Ion Battery Electrodes. *Appl. Phys. Lett.* **2017**, *110* (13), 133901. <https://doi.org/10.1063/1.4979108>.
- (104) Yang, W.; Mao, S.; Yang, J.; Shang, T.; Song, H.; Mabon, J.; Swiech, W.; Vance, J. R.; Yue, Z.; Dillon, S. J.; Xu, H.; Xu, B. Large-Deformation and High-Strength Amorphous Porous Carbon Nanospheres. *Sci. Rep.* **2016**, *6* (1), 24187. <https://doi.org/10.1038/srep24187>.
- (105) Park, M.; Zhang, X.; Chung, M.; Less, G. B.; Sastry, A. M. A Review of Conduction Phenomena in Li-Ion Batteries. *J. Power Sources* **2010**, *195* (24), 7904–7929. <https://doi.org/10.1016/j.jpowsour.2010.06.060>.
- (106) Zhang, W.; Shi, H.; Wang, D.; Wang, J.; Xiong, Z.; Wang, C.; Gu, Y.; Bai, Z.; Liang, Q.; Yan, X. Three-Dimensional Ti₃C₂ MXene@silicon@nitrogen-Doped Carbon Foam for High Performance Self-Standing Lithium-Ion Battery Anodes. *J. Electroanal. Chem.* **2022**, *921*, 116664. <https://doi.org/10.1016/j.jelechem.2022.116664>.
- (107) BoorboorAjdari, F.; Izadpanah Ostad, M.; Niknam Shahrak, M.; Ershadi, M.; Sadeghi Malek, S.; Ghasemi, F.; Zolfaghari, Y.; Ramakrishna, S. Investigating MCM-41/Metal-Organic Framework Nanocomposites as Silicon-Containing Electrodes for Supercapacitor. *Surf. Interfaces* **2022**, *29*, 101796. <https://doi.org/10.1016/j.surfin.2022.101796>.
- (108) Maiti, A.; Biswal, R.; Debnath, S.; Bhunia, A. The Energy Storage Application of Core-/Yolk-Shell Structures in Sodium Batteries. *Energy Adv.* **2024**, *3* (6), 1238–1264. <https://doi.org/10.1039/d4ya00141a>.
- (109) Gao, S.; Sun, F.; Liu, N.; Yang, H.; Cao, P.-F. Ionic Conductive Polymers as Artificial Solid Electrolyte Interphase Films in Li Metal Batteries – A Review. *Mater. Today* **2020**, *40*, 140–159. <https://doi.org/10.1016/j.mattod.2020.06.011>.
- (110) Song, H.; Lee, J.; Sagong, M.; Jeon, J.; Han, Y.; Kim, J.; Jung, H.-G.; Yu, J.-S.; Lee, J.; Kim, I.-D. Overcoming Chemical and Mechanical Instabilities in Lithium Metal Anodes with

- Sustainable and Eco-Friendly Artificial SEI Layer. *Adv. Mater.* **2024**, *36* (47), 2407381. <https://doi.org/10.1002/adma.202407381>.
- (111) Zhang, W.; Han, P.; Liu, Y.; Lin, X.; Wu, Y. Improvement Strategies and Research Progress of Silicon/Graphite Composites in Lithium-Ion Batteries. *FlatChem* **2025**, *50*, 100833. <https://doi.org/10.1016/j.flatc.2025.100833>.
- (112) Xu, C.; Shen, L.; Zhang, W.; Huang, Y.; Sun, Z.; Zhao, G.; Lin, Y.; Zhang, Q.; Huang, Z.; Li, J. Efficient Implementation of Kilogram-Scale, High-Capacity and Long-Life Si-C/TiO₂ Anodes. *Energy Storage Mater.* **2023**, *56*, 319–330. <https://doi.org/10.1016/j.ensm.2023.01.025>.
- (113) Choi, S.; Kwon, T.; Coskun, A.; Choi, J. W. Highly Elastic Binders Integrating Polyrotaxanes for Silicon Microparticle Anodes in Lithium Ion Batteries. *Science* **2017**, *357* (6348), 279–283. <https://doi.org/10.1126/science.aal4373>.
- (114) Zhang, C. (John); Park, S.-H.; Seral-Ascaso, A.; Barwich, S.; McEvoy, N.; Boland, C. S.; Coleman, J. N.; Gogotsi, Y.; Nicolosi, V. High Capacity Silicon Anodes Enabled by MXene Viscous Aqueous Ink. *Nat. Commun.* **2019**, *10* (1), 849. <https://doi.org/10.1038/s41467-019-08383-y>.
- (115) Li, Q.; Liu, X.; Han, X.; Xiang, Y.; Zhong, G.; Wang, J.; Zheng, B.; Zhou, J.; Yang, Y. Identification of the Solid Electrolyte Interface on the Si/C Composite Anode with FEC as the Additive. *ACS Appl. Mater. Interfaces* **2019**, *11* (15), 14066–14075. <https://doi.org/10.1021/acsami.8b22221>.
- (116) Jia, H.; Zou, L.; Gao, P.; Cao, X.; Zhao, W.; He, Y.; Engelhard, M. H.; Burton, S. D.; Wang, H.; Ren, X.; Li, Q.; Yi, R.; Zhang, X.; Wang, C.; Xu, Z.; Li, X.; Zhang, J.-G.; Xu, W. High-Performance Silicon Anodes Enabled By Nonflammable Localized High-Concentration Electrolytes. *Adv. Energy Mater.* **2019**, *9* (31), 1900784. <https://doi.org/10.1002/aenm.201900784>.
- (117) Nölle, R.; Achazi, A. J.; Kaghazchi, P.; Winter, M.; Placke, T. Pentafluorophenyl Isocyanate as an Effective Electrolyte Additive for Improved Performance of Silicon-Based Lithium-Ion Full Cells. *ACS Appl. Mater. Interfaces* **2018**, *10* (33), 28187–28198. <https://doi.org/10.1021/acsami.8b07683>.

- (118) Yang, X.; Tang, S.; Li, L.; He, Y.; Li, M.; Wei, X.; Hu, J.; Wang, J.; Ouyang, X.; Gu, M. D.; Zhang, Q.; Liu, J. Lithiation Depth Regulation of Silicon Anodes toward Excellent Stability. *J. Phys. Chem. Lett.* **2024**, *15* (28), 7320–7326.
<https://doi.org/10.1021/acs.jpcllett.4c01599>.
- (119) An, S. J.; Li, J.; Du, Z.; Daniel, C.; Wood, D. L. Fast Formation Cycling for Lithium Ion Batteries. *J. Power Sources* **2017**, *342*, 846–852. <https://doi.org/10.1016/j.jpowsour.2017.01.011>.
- (120) Wang, W.; Liu, W.; Wang, Y.; Gu, S.; Zheng, H. Advances in the Research of Porous Silicon Anodes for Lithium-Ion Batteries. *Chem. Eng. J.* **2025**, *523*, 168393.
<https://doi.org/10.1016/j.cej.2025.168393>.
- (121) Jin, D.; Kim, J.-M.; Yi, R.; Engelhard, M.; Xu, Y.; Baar, K.; Wang, P.; Wang, C.; Zhang, J.-G. High Performance Porous Si Anode Enabled by an Organic-Solvent Assisted Etching Process. *J. Power Sources* **2025**, *649*, 237440.
<https://doi.org/10.1016/j.jpowsour.2025.237440>.
- (122) Huanca, D. R. Porous Silicon: A Sponge-Like Structure for Photonic Based Sensor Devices. In *21st Century Nanoscience—A Handbook*; CRC Press, 2020; pp 4–1.
- (123) Karbassian, F. Porous Silicon. In *Porosity - Process, Technologies and Applications*; Ghrib, T. H., Ed.; IntechOpen: London, 2018.
<https://doi.org/10.5772/intechopen.72910>.
- (124) Yi, R.; Dai, F.; Gordin, M. L.; Chen, S.; Wang, D. Micro-Sized Si-C Composite with Interconnected Nanoscale Building Blocks as High-Performance Anodes for Practical Application in Lithium-Ion Batteries. *Adv. Energy Mater.* **2013**, *3* (3), 295–300.
<https://doi.org/10.1002/aenm.201200857>.
- (125) Kim, H.; Han, B.; Choo, J.; Cho, J. Three-Dimensional Porous Silicon Particles for Use in High-Performance Lithium Secondary Batteries. *Angew. Chem. Int. Ed.* **2008**, *47* (52), 10151–10154. <https://doi.org/10.1002/anie.200804355>.
- (126) Hesketh, P. J.; Ju, C.; Gowda, S.; Zanolari, E.; Danyluk, S. Surface Free Energy Model of Silicon Anisotropic Etching. *J. Electrochem. Soc.* **1993**, *140* (4), 1080.
<https://doi.org/10.1149/1.2056201>.

- (127) Robertson, M.; Zhou, Q.; Ye, C.; Qiang, Z. Developing Anisotropy in Self-Assembled Block Copolymers: Methods, Properties, and Applications. *Macromol. Rapid Commun.* **2021**, *42* (17), 2100300. <https://doi.org/10.1002/marc.202100300>.
- (128) Bang, B. M.; Lee, J.-I.; Kim, H.; Cho, J.; Park, S. High-Performance Macroporous Bulk Silicon Anodes Synthesized by Template-Free Chemical Etching. *Adv. Energy Mater.* **2012**, *2* (7), 878–883. <https://doi.org/10.1002/aenm.201100765>.
- (129) Xiao, Q.; Gu, M.; Yang, H.; Li, B.; Zhang, C.; Liu, Y.; Liu, F.; Dai, F.; Yang, L.; Liu, Z.; Xiao, X.; Liu, G.; Zhao, P.; Zhang, S.; Wang, C.; Lu, Y.; Cai, M. Inward Lithium-Ion Breathing of Hierarchically Porous Silicon Anodes. *Nat. Commun.* **2015**, *6* (1), 8844. <https://doi.org/10.1038/ncomms9844>.
- (130) Li, X.; Gu, M.; Hu, S.; Kennard, R.; Yan, P.; Chen, X.; Wang, C.; Sailor, M. J.; Zhang, J.-G.; Liu, J. Mesoporous Silicon Sponge as an Anti-Pulverization Structure for High-Performance Lithium-Ion Battery Anodes. *Nat. Commun.* **2014**, *5* (1), 4105. <https://doi.org/10.1038/ncomms5105>.
- (131) Ikonen, T.; Nissinen, T.; Pohjalainen, E.; Sorsa, O.; Kallio, T.; Lehto, V.-P. Electrochemically Anodized Porous Silicon: Towards Simple and Affordable Anode Material for Li-Ion Batteries. *Sci. Rep.* **2017**, *7* (1), 7880. <https://doi.org/10.1038/s41598-017-08285-3>.
- (132) SUN Peng, H. M., LI Ming-Da, MA Shuang-Yun. Microstructure, Electrical and Gas Sensing Properties of Mesoporous Silicon and Macro-Porous Silicon. *Acta Phys.-Chim. Sin.* **2012**, *28* (02), 489–493.
- (133) Jia, H.; Zheng, J.; Song, J.; Luo, L.; Yi, R.; Estevez, L.; Zhao, W.; Patel, R.; Li, X.; Zhang, J.-G. A Novel Approach to Synthesize Micrometer-Sized Porous Silicon as a High Performance Anode for Lithium-Ion Batteries. *Nano Energy* **2018**, *50*, 589–597. <https://doi.org/10.1016/j.nanoen.2018.05.048>.
- (134) Ren, Y.; Zhou, X.; Zhou, H.; Yang, J.; Chen, S.; Wu, L.; Nie, Y.; Wang, B. Zn-Assisted Magnesiothermic Reduction for the Preparation of Ultra-Fine Silicon Nanocrystals for Lithium Ion

- Batteries. *Chem. Eng. J.* **2017**, *328*, 691–696.
<https://doi.org/10.1016/j.cej.2017.07.040>.
- (135) Wu, H.; Du, N.; Shi, X.; Yang, D. Rational Design of Three-Dimensional Macroporous Silicon as High Performance Li-Ion Battery Anodes with Long Cycle Life. *J. Power Sources* **2016**, *331*, 76–81. <https://doi.org/10.1016/j.jpowsour.2016.09.046>.
- (136) Ma, J.; Zhang, H.; Liu, R.; Zhang, W.; Han, S.; Han, J.; Xu, G.; Li, L.; He, Y.-S.; Ma, Z.-F. In-Situ Processing Nano-Porous Silicon into 3D Conductive Structure as High-Capacity Anode for Lithium-Ion Batteries. *Sci. China Mater.* **2023**, *66* (2), 493–504. <https://doi.org/10.1007/s40843-022-2158-x>.
- (137) Darghouth, A.; Aouida, S.; Bessais, B. High Purity Porous Silicon Powder Synthesis by Magnesiothermic Reduction of Tunisian Silica Sand. *Silicon* **2021**, *13* (3), 667–676.
<https://doi.org/10.1007/s12633-020-00433-1>.
- (138) Wang, W.; Favors, Z.; Ionescu, R.; Ye, R.; Bay, H. H.; Ozkan, M.; Ozkan, C. S. Monodisperse Porous Silicon Spheres as Anode Materials for Lithium Ion Batteries. *Sci. Rep.* **2015**, *5* (1), 8781. <https://doi.org/10.1038/srep08781>.
- (139) Yan, N.; Wang, F.; Zhong, H.; Li, Y.; Wang, Y.; Hu, L.; Chen, Q. Hollow Porous SiO₂ Nanocubes Towards High-Performance Anodes for Lithium-Ion Batteries. *Sci. Rep.* **2013**, *3* (1), 1568.
<https://doi.org/10.1038/srep01568>.
- (140) Ma, H.; Cheng, F.; Chen, J.-Y.; Zhao, J.-Z.; Li, C.-S.; Tao, Z.-L.; Liang, J. Nest-like Silicon Nanospheres for High-Capacity Lithium Storage. *Adv. Mater.* **2007**, *19* (22), 4067–4070.
<https://doi.org/10.1002/adma.200700621>.
- (141) Tang, F.; Jiang, T.; Tan, Y.; Xu, X.; Zhou, Y. Preparation and Electrochemical Performance of Silicon@graphene Aerogel Composites for Lithium-Ion Batteries. *J. Alloys Compd.* **2021**, *854*, 157135. <https://doi.org/10.1016/j.jallcom.2020.157135>.
- (142) Li, K.; Yuan, G.; Liu, X.; Guo, Y.; Huang, R.; Li, H.; Zhang, H.; Jia, Q.; Xie, Z.; Zhang, S.; Lei, W. On the Practical Applicability of Rambutan-like SiOC Anode with Enhanced Reaction Kinetics for Lithium-Ion Storage. *Adv. Funct. Mater.* **2023**, *33* (43), 2302348. <https://doi.org/10.1002/adfm.202302348>.

- (143) Sohn, M.; Lee, D. G.; Park, H.-I.; Park, C.; Choi, J.-H.; Kim, H. Microstructure Controlled Porous Silicon Particles as a High Capacity Lithium Storage Material via Dual Step Pore Engineering. *Adv. Funct. Mater.* **2018**, *28* (23), 1800855. <https://doi.org/10.1002/adfm.201800855>.
- (144) Qu, F.; Li, C.; Wang, Z.; Wen, Y.; Richter, G.; Strunk, H. P. Eutectic Nano-Droplet Template Injection into Bulk Silicon to Construct Porous Frameworks with Concomitant Conformal Coating as Anodes for Li-Ion Batteries. *Sci. Rep.* **2015**, *5* (1), 10381. <https://doi.org/10.1038/srep10381>.
- (145) Zhou, P.; Jiang, Z.; Li, Y.; Xiao, P.; Wu, F. Sulphur-Template Method for Facile Manufacturing Porous Silicon Electrodes with Enhanced Electrochemical Performance. *Chin. Chem. Lett.* **2024**, *35* (8), 109467. <https://doi.org/10.1016/j.ccllet.2023.109467>.
- (146) Li, B.; Chuan, X.; Chen, S.; Liu, F.; Li, X. Silicon Micron Cages Derived from a Halloysite Nanotube Precursor and Aluminum Sacrificial Template in Molten AlCl₃ as an Anode for Lithium-Ion Batteries. *RSC Adv.* **2022**, *12* (32), 20850–20856. <https://doi.org/10.1039/D2RA01394K>.
- (147) Dong, H.; Fu, X.; Wang, J.; Wang, P.; Ding, H.; Song, R.; Wang, S.; Li, R.; Li, S. In-Situ Construction of Porous Si@C Composites with LiCl Template to Provide Silicon Anode Expansion Buffer. *Carbon* **2021**, *173*, 687–695. <https://doi.org/10.1016/j.carbon.2020.11.042>.
- (148) Wang, K.; Pei, S.; He, Z.; Huang, L.; Zhu, S.; Guo, J.; Shao, H.; Wang, J. Synthesis of a Novel Porous Silicon Microsphere@carbon Core-Shell Composite via in Situ MOF Coating for Lithium Ion Battery Anodes. *Chem. Eng. J.* **2019**, *356*, 272–281. <https://doi.org/10.1016/j.cej.2018.09.027>.
- (149) Gries, S.; Brinker, M.; Zeller-Plumhoff, B.; Rings, D.; Krekeler, T.; Longo, E.; Greving, I.; Huber, P. Wafer-Scale Fabrication of Hierarchically Porous Silicon and Silica by Active Nanoparticle-Assisted Chemical Etching and Pseudomorphic Thermal Oxidation. *Small* **2023**, *19* (22), 2206842. <https://doi.org/10.1002/sml.202206842>.

- (150) Becker, C. R.; Miller, D. C.; Stoldt, C. R. Galvanically Coupled Gold/Silicon-on-Insulator Microstructures in Hydrofluoric Acid Electrolytes: Finite Element Simulation and Morphological Analysis of Electrochemical Corrosion. *J. Micromechanics Microengineering* **2010**, *20* (8), 085017. <https://doi.org/10.1088/0960-1317/20/8/085017>.
- (151) Jia, H.; Gao, P.; Yang, J.; Wang, J.; Nuli, Y.; Yang, Z. Novel Three-Dimensional Mesoporous Silicon for High Power Lithium-Ion Battery Anode Material. *Adv. Energy Mater.* **2011**, *1* (6), 1036–1039. <https://doi.org/10.1002/aenm.201100485>.
- (152) Li, W.; Guo, X.; Lu, Y.; Wang, L.; Fan, A.; Sui, M.; Yu, H. Amorphous Nanosized Silicon with Hierarchically Porous Structure for High-Performance Lithium Ion Batteries. *Energy Storage Mater.* **2017**, *7*, 203–208. <https://doi.org/10.1016/j.ensm.2017.02.003>.
- (153) Shen, Y. Rice Husk Silica Derived Nanomaterials for Sustainable Applications. *Renew. Sustain. Energy Rev.* **2017**, *80*, 453–466. <https://doi.org/10.1016/j.rser.2017.05.115>.
- (154) Admase, A. T.; Asrade, E. D.; Fanta, S. W. A Comprehensive Review on Energy Storage Materials & Technologies: Applications of Nanofabrication Techniques for Enhanced Performance and Efficiency. *Mater. Renew. Sustain. Energy* **2025**, *14* (3), 56. <https://doi.org/10.1007/s40243-025-00329-3>.
- (155) Pal, P.; Swarnalatha, V.; Rao, A. V. N.; Pandey, A. K.; Tanaka, H.; Sato, K. High Speed Silicon Wet Anisotropic Etching for Applications in Bulk Micromachining: A Review. *Micro Nano Syst. Lett.* **2021**, *9* (1), 4. <https://doi.org/10.1186/s40486-021-00129-0>.
- (156) Zhu, N.; Qian, F.; Xu, X.; Wang, M.; Teng, Q. Thermogravimetric Experiment of Urea at Constant Temperatures. *Materials* **2021**, *14* (20). <https://doi.org/10.3390/ma14206190>.
- (157) Tischer, S.; Börnhorst, M.; Amsler, J.; Schoch, G.; Deutschmann, O. Thermodynamics and Reaction Mechanism of Urea Decomposition. *Phys. Chem. Chem. Phys.* **2019**, *21* (30), 16785–16797. <https://doi.org/10.1039/C9CP01529A>.

- (158) Galakhova, A.; Kadisch, F.; Mori, G.; Heyder, S.; Wieser, H.; Sartory, B.; Burger, S. Corrosion of Stainless Steel by Urea at High Temperature. *Corros. Mater. Degrad.* **2021**, *2* (3), 461–473. <https://doi.org/10.3390/cmd2030024>.
- (159) Hamm, D.; Sakka, T.; Ogata, Y. H. Etching of Porous Silicon in Basic Solution. *Phys. Status Solidi A* **2003**, *197* (1), 175–179. <https://doi.org/10.1002/pssa.200306495>.
- (160) Pal, P.; Sato, K. *Silicon Wet Bulk Micromachining for MEMS*; Jenny Stanford Publishing, 2017.
- (161) Zubov, D. N.; Sokolov, S. A. Catalytic Etching of Silicon in Solutions Containing Hydrazine. *Inorg. Mater. Appl. Res.* **2025**, *16* (2), 298–303. <https://doi.org/10.1134/S2075113324701661>.
- (162) Fundamentals of Porous Silicon Preparation. In *Porous Silicon in Practice*; 2011; pp 1–42. <https://doi.org/10.1002/9783527641901.ch1>.
- (163) Kern, W. Chemical Etching of Silicon, Germanium, Gallium Arsenide, and Gallium Phosphide. **1978**.
- (164) Zhou, M.; Chen, M. Reactions of Silicon Dioxide with Ammonia Molecules: Formation and Characterization of the SiO₂–NH₃ Complex and the H₂NSiOOH Molecule. *Chem. Phys. Lett.* **2001**, *349* (1), 64–70. [https://doi.org/10.1016/S0009-2614\(01\)01192-7](https://doi.org/10.1016/S0009-2614(01)01192-7).
- (165) Chen, W.; Fan, Z.; Dhanabalan, A.; Chen, C.; Wang, C. Mesoporous Silicon Anodes Prepared by Magnesiumthermic Reduction for Lithium Ion Batteries. *J. Electrochem. Soc.* **2011**, *158* (9), A1055. <https://doi.org/10.1149/1.3611433>.
- (166) Scherrer, P. Bestimmung Der Grosse Und Inneren Struktur von Kolloidteilchen Mittels Rontgenstrahlen. *Nach Ges Wiss Gottingen* **1918**, *2*, 8–100. https://doi.org/10.1007/978-3-662-33915-2_7.
- (167) Kharin, A. Y.; Kargina, Y. V.; Timoshenko, V. Y. Evolution of Nanocrystal Size Distribution in Porous Silicon Nanoparticles during Storage in Aqueous Media: X-Ray Diffraction Analysis. *J. Nanoparticle Res.* **2019**, *21* (2), 27. <https://doi.org/10.1007/s11051-019-4466-9>.

- (168) Romanitan, C.; Kusko, M.; Popescu, M.; Varasteanu, P.; Radoi, A.; Pachiu, C. Unravelling the Strain Relaxation Processes in Silicon Nanowire Arrays by X-Ray Diffraction. *Appl. Crystallogr.* **2019**, *52* (5), 1077–1086.
<https://doi.org/10.1107/S1600576719010707>.
- (169) Kumar, R.; Tanwar, M. Effect of Some Physical Perturbations and Their Interplay on Raman Spectral Line Shapes in Silicon: A Brief Review. *J. Raman Spectrosc.* **2021**, *52* (12), 2100–2118.
<https://doi.org/10.1002/jrs.6272>.
- (170) Hamdi, A.; Amri, C.; Ouertani, R.; Ezzaouia, H. Effect of Etching Time on Morphological, Optical and Structural Properties of Silicon Nanowire Arrays Etched on Multi-Crystalline Silicon Wafer. *J. Mater. Sci. Mater. Electron.* **2017**, *28* (6), 4807–4813. <https://doi.org/10.1007/s10854-016-6126-5>.
- (171) Ossadnik, C.; Vepřek, S.; Gregora, I. Applicability of Raman Scattering for the Characterization of Nanocrystalline Silicon. *Thin Solid Films* **1999**, *337* (1), 148–151.
[https://doi.org/10.1016/S0040-6090\(98\)01175-4](https://doi.org/10.1016/S0040-6090(98)01175-4).
- (172) Veprek, S.; Sarott, F.-A.; Iqbal, Z. Effect of Grain Boundaries on the Raman Spectra, Optical Absorption, and Elastic Light Scattering in Nanometer-Sized Crystalline Silicon. *Phys. Rev. B* **1987**, *36* (6), 3344–3350.
<https://doi.org/10.1103/PhysRevB.36.3344>.
- (173) Park, J. S.; Lee, J. M.; Hwang, S. K.; Lee, S. H.; Lee, H.-J.; Lee, B. R.; Park, H. I.; Kim, J.-S.; Yoo, S.; Song, M. H.; Kim, S. O. A ZnO/N-Doped Carbon Nanotube Nanocomposite Charge Transport Layer for High Performance Optoelectronics. *J. Mater. Chem.* **2012**, *22* (25), 12695–12700.
<https://doi.org/10.1039/C2JM30710C>.
- (174) Hwang, S. M.; Kim, H. S.; Le, D. N.; Ravichandran, A. V.; Sahota, A.; Lee, J.; Jung, Y. C.; Kim, S. J.; Ahn, J.; Hwang, B. K.; Lee, L.; Zhou, X.; Kim, J. Plasma-Enhanced Atomic-Layer Deposition of Nanometer-Thick SiNx Films Using Trichlorodisilane for Etch-Resistant Coatings. *ACS Appl. Nano Mater.* **2021**, *4* (3), 2558–2564.
<https://doi.org/10.1021/acsanm.0c03203>.

- (175) Ghosh, R.; Gopalakrishnan, S.; Renganathan, T.; Pushpavanam, S. Adsorptive Colorimetric Determination of Chromium(VI) Ions at Ultratrace Levels Using Amine Functionalized Mesoporous Silica. *Sci. Rep.* **2022**, *12* (1), 5673.
<https://doi.org/10.1038/s41598-022-09689-6>.